Coupling Factor Estimation for Electrical Vehicles Wireless Charging

H. Song

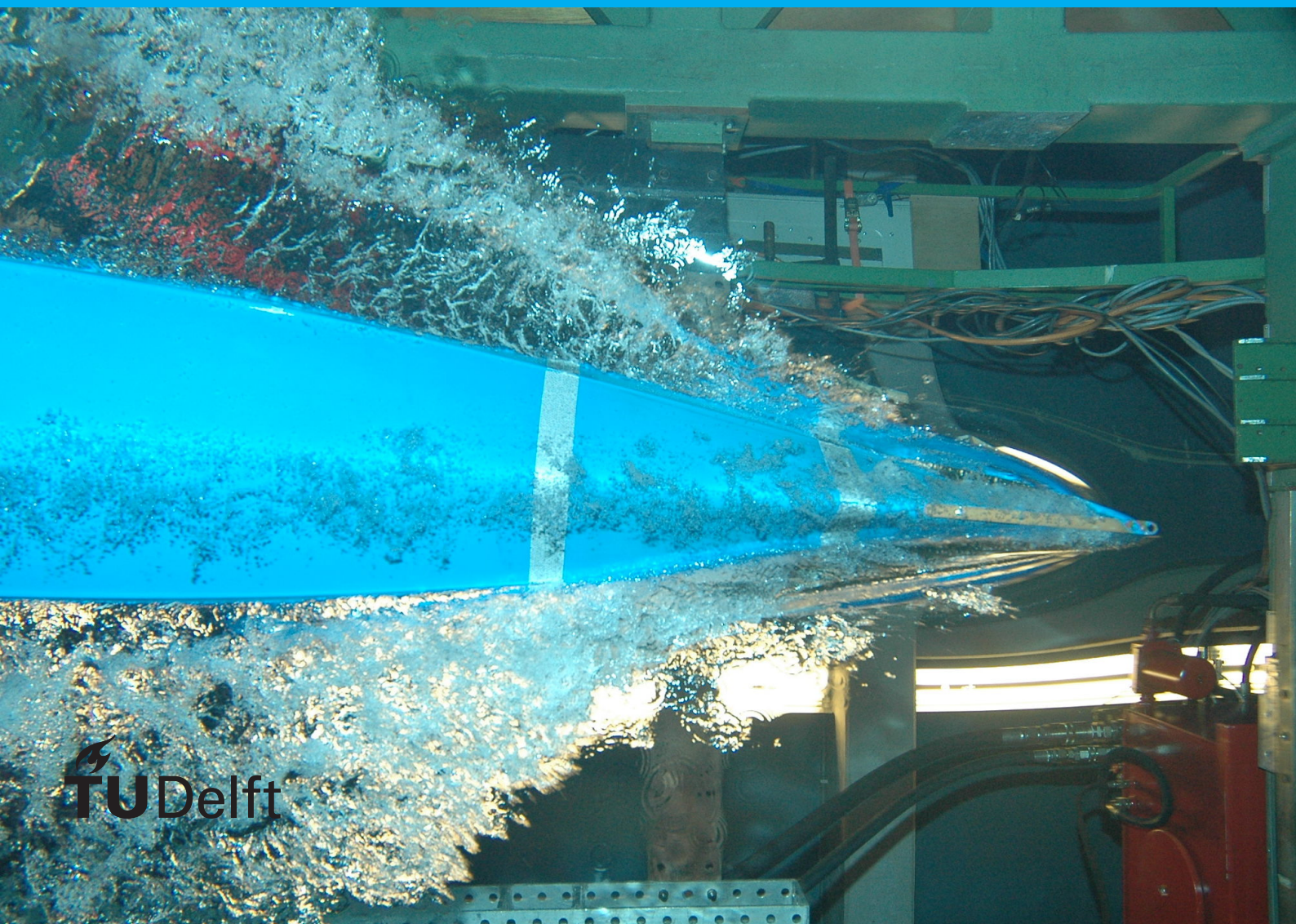

Coupling Factor Estimation for Electrical Vehicles Wireless Charging

by

H. Song

to obtain the degree of Master of Science
at the Delft University of Technology,
to be defended publicly on Thursday September 15, 2022 at 15:30 PM.

Student number:	5346592	
Project duration:	November 1, 2021 – September 15, 2022	
Daily supervisor:	Dr. J. Dong,	TU Delft
	Dr. C. Riekerk,	TU Delft
Thesis committee:	Prof. dr. P. Bauer,	TU Delft, supervisor
	Dr. J. Dong,	TU Delft, daily supervisor
	Dr. M. Milos Cvetkovic,	TU Delft

TU Delft

Preface

This thesis “Coupling Factor Estimation for Electrical Vehicles Wireless Charging” has been written to meet the requirement to obtain the ”Master of Science” degree at the Delft University of technology.
I could not have completed this thesis without the support of many people. So I want to show my gratitude to these people. First, I want to thank my daily supervisor, Jianning. You have taught me a lot about the PLL unit and provided many advice and feedback on my thesis.
Next, I want to thank my another daily supervisor, Calvin. At the start of the project, you have given me many suggestions about my thesis and have taught me many things about simulation tools.
Then, I want to thank my friends and classmates. They provided much help for me when I got trouble with my studies. Riding with them on weekend also lets me relax. Lastly, I want to thank my parents. They always support me in chasing my dream.

H. Song
Delft, September 2022

abstract

With the popularity of electrical vehicles (EVs), the demand for EVs charging is also increased. Compared to traditional wired charging, wireless charging can avoid many safety issues. The efficiency of wireless power transfer (WPT) system is determined by many factors, the coupling factor is one of the most important factors. Therefore, estimating the coupling factor of WPT system is necessary. The research objectives of this work are to review and benchmark different methodology of coupling factor estimation. Besides, a comprehensive method is selected and simulated.

This work is focused on magnetic inductive WPT systems. Five different methodologies of coupling factor estimation for static WPT system and one methodology for dynamic WPT system is reviewed and analyzed. The methodology that uses alternative capacitors to estimate the coupling factor of a static WPT system is analyzed in detail. By using the zero crossing unit, the primary side and secondary side of WPT system are under full resonant. The WPT system will work in two different modes by changing the primary side capacitance. The two sets of circuit parameters will be recorded and calculated by a PLL unit. Based on theoretical analysis and the calculated parameter, the load and mutual inductance of WPT system can be identified. Therefore, the value of the coupling factor can be determined. The accuracy of coupling factor estimation of this methodology is higher than 97 %.

Compared to the literature that proposed this methodology, this work made a sensitivity study. The circuit parameters is made to fluctuate in a certain range. The accuracy of estimation of mutual inductance is still higher than 95% when the primary side resistance, secondary side resistance and load fluctuate. However, the system becomes unstable when the primary side capacitance, inductance and secondary side inductance fluctuate. The reason is that when the capacitance and inductance change, the operating frequency will deviate from the resonant frequency. However, the mutual inductance identification unit is not able to detect this deviation. If the deviation of circuit parameters is updated, the accuracy of coupling factor estimation will remain at about 97%.

Contents

1

Introduction

In recent years, electric vehicles (EVs) have become more and more popular because of the trend of lower carbon emissions.Therefore, the demands for vehicle charging are increasing. At present, wired charging is the mainstream charging method for electrical vehicles because of its high stability, efficiency and inexpensive nature. However, there are still some drawbacks of high power wired charging, for example, sparks may be produced during plugging, carbon deposition and short service life. As an innovative solution, wireless power transfer (WPT) can efficiently avoid these problems[1] [2] because of the absence of physical connection and wear. The definition of wireless power transfer is the electrical power transfer from the transmitter to the receiver without a wired connection. The transmitting coil is connected to the dc power source through a DC-AC inverter. The AC current will generate a varying magnetic field in the transmitting coil. The power will be transferred from the transmitter to the receiver through the varying magnetic field. The receiving coil is connected to the load and supplies the power to the load. Wireless power transfer can avoid using wires and sockets and improve safety issues, reliability issue, low maintenance and long product life[3] [4]. Besides, this technology provides more convenience for EVs driver when they try to charge their vehicles.[5]

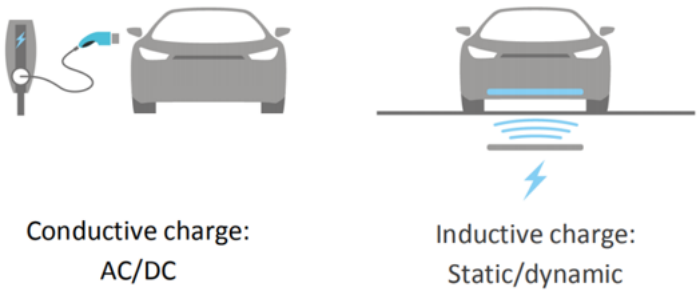

Figure 1.1: Conductive charging and inductive charging for EVs

1.1. Wireless power transfer

Wireless power transfer systems can be also classified into three different categories based on the transfer mechanism[1]:

1. Electromagnetic radiation
2. Electric coupling
3. Electromagnetic induction

The relationship between the different WPT systems is shown in Figure 1.2. Electric coupling WPT system is also called capacitive WPT system. The electric coupling WPT system sets metal plate electrodes at the transmitter and the receiver at the same time, and realizes wireless charging through the electric field between two metal plates. Compared with the electromagnetic WPT technology, the effective transmission range of the electric coupling WPT system is much less [1]. Therefore, capacitive

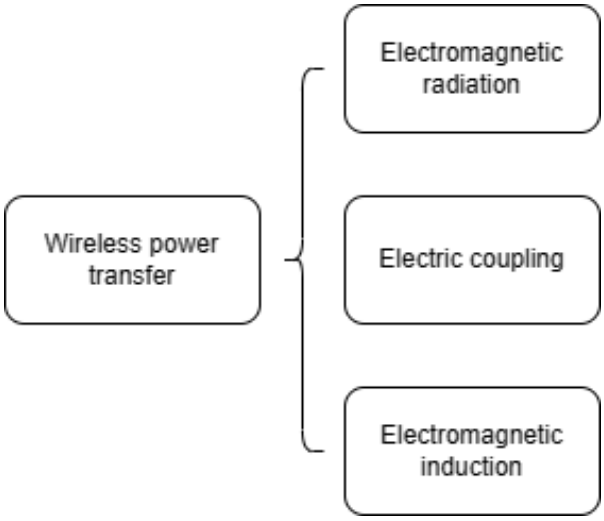

Figure 1.2: Different categories of WPT system(based on the mechanism)

WPT system is not suitable for EVs wireless charging.

Electromagnetic radiation technology is characterized by long-distance transmission, however, its transmission efficiency is very limited compared to electromagnetic WPT technology [1]. The main requirement for EVs wireless power transfer is high power and high efficiency. Therefore, electromagnetic radiation technology is rarely applied in EVs wireless charging.

Due to the limitations of the WPT system mentioned above, the electromagnetic induction WPT system has become the most common WPT system for EVs wireless charging at present [1]. It realizes energy transmission based on the principle of electromagnetic induction.

According to Ampere's law, a magnetic field around the wire will be built when there is an AC current on the primary side. As a result, a time varying magnetic field is built. The magnetic coupler in the secondary side will be coupled with the time varying magnetic field.

$$\oint_C H\,dl = I + I_d \tag{1.1}$$

Where H is the magnetic field intensity, I is the current of the conductor, I_d is the displacement current.

According to Faraday's law, a voltage will be induced in the secondary side.

$$\oint_C E\,dl = -\frac{\delta\phi}{\delta t} \tag{1.2}$$

Where E is , ϕ is the time varying magnetic flux.

This induced voltage can be converted to DC signal by the rectifier. The schematic of this power transfer system is shown in Figure 1.3.

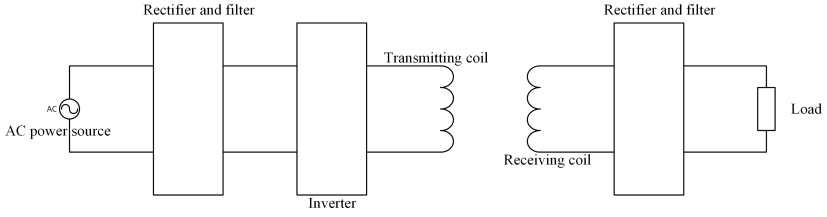

Figure 1.3: General schematic of a inductive WPT system

Magnetic resonant coupling wireless power transfer system is a kind of inductive wireless power transfer system. Similar to the traditional inductive WPT system, the voltage on the secondary side is induced by the magnetic field on the primary side. This induced voltage can be converted to the DC signal. Compared to the traditional inductive WPT system, the compensation network on the primary side and the secondary side are resonated with each other when they work in the same resonant frequency. The detail of the compensation network will be introduced in the next subsection. The different typologies of the compensation networks will cause different output properties of the system. The power transfer and magnetic coupling will be enhanced because of the resonant coils [6].

For inductive WPT systems for EVs, the charging methods can be classified as static wireless charging and dynamic wireless charging. For the static cases, EVs are required to be parked. For the dynamic cases, EVs are in motion [7].

1.2. Standard

With the popularity of wireless charging for EVs, it is necessary to establish standards to ensure safety and universality. At present, there are three commonly used standards for EVs wireless charging, IEC 61980-1, ISO 19363 and SAE J2954 RP.

1.2.1. IEC 61980-1

This standard provides the requirement for electrical safety, electromagnetic compatibility(EMC) and electromagnetic field exposure(EMF) [8].

Based on series IEC 61000, IEC 61980 provided the requirement for immunity and conducted disturbances for EMC. The regulation of EMF for humans is based on the ICNIRP's guidelines [9]. It protects against all known bad health effect on human.

1.2.2. ISO 19363

This standard involves the requirements for safety and interoperability for wireless power transfer for passenger vehicles [10]. Besides, it also provides some requirements about operating frequency and frequency. The efficiency of the wireless power transfer system should be above 85% if there is no misalignment between the primary side and the secondary side. If there is a misalignment between the primary side and the secondary side, the minimum efficiency should be above 80 %. The operating frequency should range from 81.38 kHz to 90 kHz.

This standard does not provide an EMC regulation but refers to CISPR/D. For EMF regulation, it provides two protection levels. One is based on ICNIRP Guideline, which protects humans from electromagnetic fields, and another one is based on ISO 14117-1 which is focus on active implantable medical device security.

1.2.3. SAE J2954 RP

This standard is set for the case of static and unidirectional passengers EVs wireless charging [11]. It also includes some requirement for operating frequency. The operating frequency should range from 79 kHz to 90 kHz. This standard set the WPT power class for the WPT systems in different power levels. The information is shown in Table 1.1.

Table 1.1: Efficiency requirements for different power levels for WPT [11].

	WPT Power Class			
	WPT1	WPT2	WPT3	WPT4
Maximum input VA	3.7 kVA	7.7 kVA	11.1 kVA	22 kVA
Minimum target efficiency when alignment	>85%	>85%	>85%	TBD in next phase
Minimum target efficiency when misalignment	>80%	>80%	>80%	TBD in next phase
EMC limit	67.8 dB	67.8 dB	82.8 db	TBD in next phase

This standard also involves foreign object detection. The system should be off if a foreign object is detected. Besides, in the case no foreign object is detected, the system should monitor the temperature of the primary side and keep it under a rated temperature. In addition, if nearby living beings are

detected, the system should adjust itself to make sure the magnetic field is not a hazard for living beings.

The EMC limit is 67.8 dB for WPT1 and WPT2. For WPT3 is 82.8 dB. The general limit for EMF is also based on ICNIRP Guideline 2010, just like in ISO 19363. The EMF for active implantable medical devices is based on AAMI/ISO 14117-2012. Furthermore, efficiency targets are set for different power levels. In Table 1.1 the efficiency requirements are shown. The requirements for WPT4 still need to be decided upon. Moreover, an efficiency of 75% is required for power classes that are not listed in this table. This gives an example of why it is important to have soft-switching for the inverter as it could help the system to reach more easily the listed efficiency requirement from this standard by reducing the switching losses in the inverter.

1.3. Compensation

In order to analyze the wireless power transfer system at the circuit level, the compensation network of the primary side and the secondary side is necessary to be studied. In this chapter, basic compensation and double-sided LCC compensation will be introduced and compared.

1.3.1. Basic compensations

There are four types of basic compensation: series-series compensation, series-parallel compensation, parallel-series compensation and parallel-parallel compensation. These typologies are shown in this subsection.

The first topology is series to series compensation.

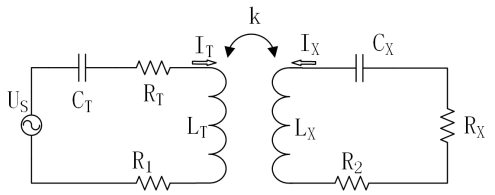

Figure 1.4: The equivalent circuit of a series-series compensated WPT system

The resonant frequency is

$$\omega_0 = \frac{1}{\sqrt{L_T C_T}} = \frac{1}{\sqrt{L_X C_X}} \tag{1.3}$$

According to the Kirchhoff law,

$$U_s = (R_T + R_1 + j\omega L_T + \frac{1}{j\omega C_T})I_T - j\omega M I_X \tag{1.4}$$

$$0 = -j\omega M I_T + (R_2 + R_x + j\omega L_X + \frac{1}{j\omega C_x})I_X \tag{1.5}$$

Let

$$Z_1 = R_1 + R_T + j\omega L_T + \frac{1}{j\omega C_T} \tag{1.6}$$

$$Z_2 = R_2 + R_X + j\omega L_X + \frac{1}{j\omega C_X} \tag{1.7}$$

The current through R_X of this topology is

$$I_X = \frac{-j\omega M U_S}{\omega^2 M^2 + Z_1 Z_2} \tag{1.8}$$

The output voltage of this topology is

$$U_X = I_X R_X = \frac{-j\omega M U_S}{\omega^2 M^2 + Z_1 Z_2} R_x \tag{1.9}$$

The effective output power is

$$P_o = \frac{|I_X|^2}{2} R_X = \frac{\omega^2 M^2 U_S^2}{2(\omega^2 M^2 + Z_1 Z_2)^2} R_X \tag{1.10}$$

The efficiency of this topology is

$$\eta = \frac{P_o}{P_i} = \frac{|I_x|^2 \frac{R_x}{2}}{\frac{|I_T|^2 Z_1}{2} + \frac{|I_X|^2 Z_2}{2}} \times 100\% = \frac{\omega^2 M^2 R_X}{Z_1^2 Z_2^2 + \omega^2 M^2 Z_2} \times 100\% \tag{1.11}$$

In practical applications, SS and SP compensation are most commonly used because of their higher efficiency [12][13]. Besides, SS topology also has the advantage that the compensation capacities are not dependent on coupling factor and resonance frequency [14][15].

The second topology is series to parallel compensation.

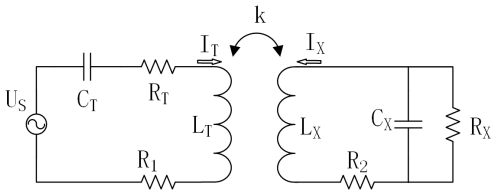

Figure 1.5: The equivalent circuit of a series-parallel compensated WPT system

The resonant frequency is

$$\omega_0 = \frac{1}{\sqrt{(L_T - \frac{M^2}{L_X})C_T}} = \frac{1}{\sqrt{L_X C_X}} \tag{1.12}$$

According to the Kirchhoff law,

$$U_s = (R_T + R_1 + j\omega L_T + \frac{1}{jC_T})I_T - j\omega M I_X \tag{1.13}$$

$$0 = -j\omega M I_T + (R_2 + R_X + j\omega L_X + \frac{\frac{1}{j\omega C_X} R_X}{\frac{1}{j\omega C_X} + R_X})I_X \tag{1.14}$$

Let

$$Z_1 = R_1 + R_T + j\omega L_T + \frac{1}{j\omega C_T} \tag{1.15}$$

$$Z_2 = R_2 + R_X + j\omega L_X + \frac{\frac{1}{j\omega C_X} R_X}{\frac{1}{j\omega C_X} + R_X} \tag{1.16}$$

The current through R_X of this topology is

$$I_X = \frac{-j\omega M U_S}{(\omega^2 M^2 + Z_1 Z_2)\sqrt{(1 + j\omega C_X R_X)}} \tag{1.17}$$

The output voltage of this topology is

$$U_X = I_X R_X = \frac{-j\omega M U_S}{(\omega^2 M^2 + Z_1 Z_2)\sqrt{(1 + j\omega C_X R_X)}} R_X \tag{1.18}$$

The effective output power is

$$P_o = \frac{|I_X|^2}{2} R_X = \frac{\omega^2 M^2 U_S^2}{2(\omega^2 M^2 + Z_1 Z_2)^2 (1 + j\omega C_X R_X)} R_X \tag{1.19}$$

The efficiency of this topology is

$$\eta = \frac{P_o}{P_i} = \frac{R_X}{(\omega^2 + \frac{Z_1 Z_2}{M^2})^2 (R_X - \frac{j}{C_2 \omega})^2 C_2^2 Z_2} \times 100\% \tag{1.20}$$

The third topology is parallel to series compensation.

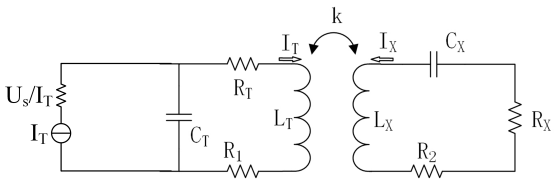

Figure 1.6: The equivalent circuit of a parallel-series compensated WPT system

The resonant frequency is

$$\omega_0 = \frac{1}{\sqrt{L_T C_T}} = \frac{1}{\sqrt{L_X C_X}} \tag{1.21}$$

(1.22)

According to the Kirchhoff law,

$$U_S = \frac{\frac{1}{j\omega C_T}(R_1 + R_T + j\omega L_T)}{\frac{1}{j\omega C_T} + R_1 + R_T + j\omega L_T} I_T - j\omega M I_X \tag{1.23}$$

$$0 = -j\omega M I_T + (R_2 + R_X + j\omega L_X + \frac{1}{j\omega C_X}) I_X \tag{1.24}$$

Let

$$Z_1 = \frac{\frac{1}{j\omega C_T}(R_1 + R_T + j\omega L_T)}{\frac{1}{j\omega C_T} + R_1 + R_T + j\omega L_T} \tag{1.25}$$

$$Z_2 = R_2 + R_X + j\omega L_X + \frac{1}{j\omega C_X} \tag{1.26}$$

The current through R_X of this topology is

$$I_X = \frac{U_S \omega M}{(Z_1 Z_2 + (\omega M)^2)^2} \tag{1.27}$$

The output voltage of this topology is

$$U_X = I_X R_X = \frac{U_S \omega M}{(Z_1 Z_2 + (\omega M)^2)^2} R_X \tag{1.28}$$

The effective output power is

$$P_o = \frac{|I_X|^2}{2} R_X = \frac{\omega^2 M^2 U_S^2}{2(\omega^2 M^2 + Z_1 Z_2)^2} R_X \tag{1.29}$$

The efficiency of this topology is

$$\eta = \frac{P_o}{P_i} = \frac{\omega^2 M^2 R_X}{Z_1^2 Z_2^2 + \omega^2 M^2 Z_2} \times 100\% \tag{1.30}$$

The fourth topology is parallel to parallel compensation.

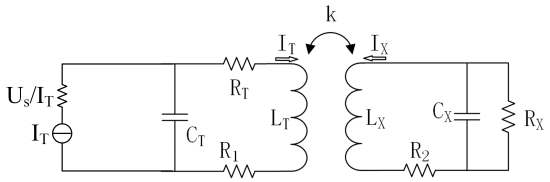

Figure 1.7: The equivalent circuit of a parallel-parallel compensated WPT system

The resonant frequency is

$$\omega_0 = \frac{1}{\sqrt{(L_T - \frac{M^2}{L_X})C_T}} = \frac{1}{\sqrt{L_X C_X}} \tag{1.31}$$

(1.32)

According to the Kirchhoff law,

$$U_S = \frac{\frac{1}{j\omega C_T}(R_1 + R_T + j\omega L_T)}{\frac{1}{j\omega C_T} + R_1 + R_T + j\omega L_T} I_T - j\omega M I_X \tag{1.33}$$

$$0 = -j\omega M I_T + (R_2 + R_X + j\omega L_X + \frac{\frac{1}{j\omega C_X} R_X}{\frac{1}{j\omega C_X} + R_X}) I_X \tag{1.34}$$

Let

$$Z_1 = \frac{\frac{1}{j\omega C_T}(R_1 + R_T + j\omega L_T)}{\frac{1}{j\omega C_T} + R_1 + R_T + j\omega L_T} \tag{1.35}$$

$$Z_2 = R_2 + R_X + j\omega L_X + \frac{\frac{1}{j\omega C_X} R_X}{\frac{1}{j\omega C_X} + R_X} \tag{1.36}$$

The current through R_X of this topology is

$$I_X = \frac{-j\omega M U_S}{(\omega^2 M^2 + Z_1 Z_2)\sqrt{(1 + j\omega C_X R_X)}} \tag{1.37}$$

The output voltage of this topology is

$$U_X = I_X R_X = \frac{-j\omega M U_S}{(\omega^2 M^2 + Z_1 Z_2)\sqrt{(1 + j\omega C_X R_X)}} R_X \tag{1.38}$$

(1.39)

The effective output power is

$$P_o = \frac{|I_X|^2}{2} R_X = \frac{\omega^2 M^2 U_S^2}{2(\omega^2 M^2 + Z_1 Z_2)^2 (1 + j\omega C_X R_X)} R_X \tag{1.40}$$

The efficiency of this topology is

$$\eta = \frac{P_o}{P_i} = \frac{R_X}{(\omega^2 + \frac{Z_1 Z_2}{M^2})^2 (R_X - \frac{j}{C_2 \omega})^2 C_2^2 Z_2} \times 100\% \tag{1.41}$$

1.3.2. Complex compensation

There are many complex compensations network for WPT systems, for example, LCL and LCC. Complex compensation network have similar properties as basic compensation but with more controllable parameters. This section will take the LCC compensation network as an example to analyze. Literature [16] has discussed the equivalent circuit of dual side LCC compensation. The equivalent circuit is shown in Figure 1.8.

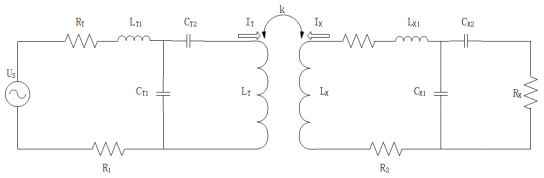

Figure 1.8: The equivalent circuit of a dual-side LCC compensated WPT system

The resonant frequency is

$$\omega_0 = \frac{1}{\sqrt{((L_P - L_1)C_1}} = \frac{1}{\sqrt{((L_S - L_2)C_2}} = \frac{1}{\sqrt{(L_1 C_3}} = \frac{1}{\sqrt{L_2 C_4}} \tag{1.42}$$

According to the Kirchhoff law,

$$(j\omega L_1 + \frac{1}{j\omega C_3})i_{f1} - \frac{1}{j\omega C_3} i_P = U_{AB} \tag{1.43}$$

$$(j\omega L_P + \frac{1}{j\omega C_1})i_P - \frac{1}{j\omega C_3} i_{f1} - jMi_S = 0 \tag{1.44}$$

$$(j\omega L_S + \frac{1}{j\omega C_2})i_S - \frac{1}{j\omega C_4} i_{f2} - jMi_P = 0 \tag{1.45}$$

$$(j\omega L_2 + \frac{1}{j\omega C_4} + R_e)i_{f2} - \frac{1}{j\omega C_4} i_S = 0 \tag{1.46}$$

Therefore, i_S and i_P can be derived as below.

$$i_S = \frac{j\omega M(j\omega L_2 + \frac{1}{j\omega C_4} + R_e)}{(j\omega L_2 + \frac{1}{j\omega C_4} + R_e)(j\omega L_S + \frac{1}{j\omega C_2}) - (\frac{1}{j\omega C_4})^2} i_P \tag{1.47}$$

$$i_P = \frac{U_{AB}(-\frac{1}{j\omega C_3})}{(\frac{1}{j\omega C_3})^2 - (j\omega L_P + \frac{1}{j\omega C_1})(j\omega L_1 + \frac{1}{j\omega C_3}) + j\omega M(j\omega L_1 + \frac{1}{j\omega C_3})\frac{j\omega M(j\omega L_2 + \frac{1}{j\omega C_4} + R_e)}{(j\omega L_2 + \frac{1}{j\omega C_4} + R_e)(j\omega L_S + \frac{1}{j\omega C_2}) - (\frac{1}{j\omega C_4})^2}} \tag{1.48}$$

Where i_P is the current through the primary side, i_S is the current through the secondary side.

The output voltage of this topology is

$$U_X = I_X R_X = \frac{j\omega M(j\omega L_2 + \frac{1}{j\omega C_4} + R_e)}{(j\omega L_2 + \frac{1}{j\omega C_4} + R_e)(j\omega L_S + \frac{1}{j\omega C_2}) - (\frac{1}{j\omega C_4})^2} i_P R_X \tag{1.49}$$

(1.50)

The effective output power is

$$P_o = \frac{|I_S|^2}{2} R_X = \left| \frac{j\omega M(j\omega L_2 + \frac{1}{j\omega C_4} + R_e)}{4(j\omega L_2 + \frac{1}{j\omega C_4} + R_e)(j\omega L_S + \frac{1}{j\omega C_2}) - (\frac{1}{j\omega C_4})^2} i_P \right|^2 R_X \tag{1.51}$$

Table 1.2: Summary of different compensation network

	SS	SP	PS	PP	Dual-LCC
Dependency on the load	Capacitances of the primary side and the secondary side are independent on the load	Capacitances of the secondary side are dependent on the load	Capacitances of the primary side are dependent on the load	Capacitances of the secondary side are dependent on the load	Not dependent on the load
Dependency on the coupling coefficient	Capacitances of the primary side and the secondary side are independent on the coupling coefficient	Capacitances of the secondary side are dependent on the coupling factor	Capacitances of the primary side are dependent on the coupling factor	Capacitances of the secondary side are dependent on the coupling factor	Not dependent on the coupling factor
Load independent output	Voltage and current	Voltage and current	Voltage	Current	Voltage and current
Sensitivity to misalignment	Slightly sensitivity	Moderate	High	High	High
Other advantages	Higher efficiency than SP (f >1 MHz)	Requires smaller self-inductance of secondary side coil	\	\	Low current stress on the inverter
Disadvantages	1.Requires larger receiver coil 2.Requires higher voltage tolerance of capacitors	Less DC component blocking	Requires high driving voltage when transferring high power	1.Requires high voltage for high power applications 2.Low power factor and high load voltage	Complex topology

The efficiency of this topology is

$$\eta = \frac{P_o}{P_i} = \frac{\left|\frac{j\omega M(j\omega L_2+\frac{1}{j\omega C_4}+R_e)}{(j\omega L_2+\frac{1}{j\omega C_4}+R_e)(j\omega L_S+\frac{1}{j\omega C_2})-(\frac{1}{j\omega C_4})^2} i_P\right|^2}{2} R_X}{U_{AB} I_P} = \frac{\left|\frac{j\omega M(j\omega L_2+\frac{1}{j\omega C_4}+R_e)}{(j\omega L_2+\frac{1}{j\omega C_4}+R_e)(j\omega L_S+\frac{1}{j\omega C_2})-(\frac{1}{j\omega C_4})^2}\right|^2 i_P R_X}{2U_{AB}} \times 100\% \tag{1.52}$$

The summary of these compensations network is shown in Table 1.2.

In order to optimize the transmission performance of the WPT system, a parametric optimization is necessary before being in production [17].

The efficiency of a WPT system is governed by many factors, such as the coupling factor between the primary side and the secondary side, the quality factors of transmitting coils and receiving coils, operating frequency and impedance matching conditions [18]. Take the compensation analysis in section 1.3 as an example, the transfer efficiency of a wireless power systems is dependent on primary side impedance, secondary impedance, efficiency and mutual inductance. When the mutual inductance and primary side impedance is fixed, there is an optimized load for maximum transfer efficiency. The circuit parameters are known parameters except for the mutual inductance. Therefore, to estimate the mutual inductance is a necessary work for system optimization.

In real life, the performance of a WPT system is highly sensitive to parameter variation, for example, self-inductance and mutual inductance will alter due to different displacements caused by arbitrary parking and different air gaps affected by chassis height and tire pressure as shown in Figure 1.9 [19].

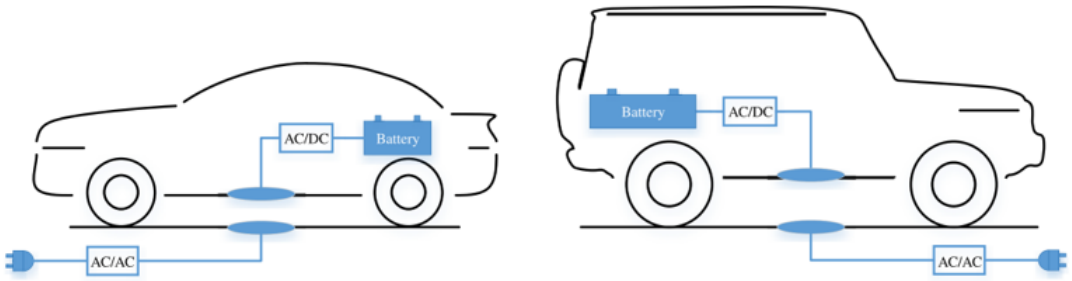

Figure 1.9: Wireless charging for EVs

Besides, the status of the batteries of different vehicles will also influences the load impedance and coupling factor. If the operating frequency of the WPT system will not change with the coupling factor and load impedance, the high efficient WPT wireless charging is not guaranteed.

Therefore, estimating the coupling factor accurately is necessary and essential to optimize the transmission efficiency for EVs wireless charging.

1.4. Research objective

This thesis focuses on the coupling factor of the magnetic resonant coupling WPT system. The research objectives of the thesis are:

- To review and classify the detection systems used to estimate the magnetic coupling factor for both static and dynamic EVs wireless charging.
- To benchmark the selected method with other coupling-estimation methods.
- To implement the proof of concept of the selected approach in the simulation tools.

1.5. Thesis structure

The thesis structure is shown below:
The background information, for example, the wireless charging standard and the typologies compensation network will be introduced in Chapter 1. Besides, the research objectives and thesis outline will also be introduced in Chapter 1. In Chapter 2, the definition of the coupling factor and the existing technology of coupling factor estimation will be introduced. Theoretical review and comparison will be implemented in this chapter. Besides, the simulation of particular methods will also be implemented in Chapter 3. Chapter 4 is the sensitivity study for the selected method. In this Chapter, the stability of the system will be discussed. Chapter 5 is the summary of this thesis, and future work will also be introduced in this chapter.

2

Existing coupling factor estimation methodology

2.1. Coupling factor

The coupling factor is an essential parameter for a WPT system. The coupling coefficient is the ratio of the open-circuit actual voltage ratio to the ratio that would be obtained if all the flux coupled from one magnetic circuit to the other. The coupling coefficient can be represented by the formula 2.1:

$$k = \frac{M}{\sqrt{L_1 L_2}} \tag{2.1}$$

Where k is the coupling factor, M is the mutual inductance, L_1 is the inductance of the first coil and L_2 is the inductance of the second coil.
The efficiency of a WPT system is depended on mutual inductance between the transmitting side and receiving side, quality factors of the coils and resonant frequency, etc. Therefore, to estimate the coupling factor accurately is important to assess a WPT system.

2.2. Existing methodology

At present, existing coupling factor estimation methodology can be divided into two different categories as shown in Figure 2.1. The first category is for the static case and the second category is for the dynamic case. Static case means the receivers will not move when being charged and the dynamic case means the receivers will move when being charged.

This thesis is mainly focused on the static case. For static cases, the existing methodology can be classified into three different categories
1. Using information from the primary side.
2. Using information from the secondary side.
3. Using information from both two sides.

The information of the primary side or the secondary side can be the measured value, for example, current, voltage and frequency. It can also be the circuit parameter, such as the resistance.

Some typical methodologies will be introduced below.

[20] proposed a method that can estimate the secondary side information and mutual inductance by using the primary side information. The circuit topology is shown in Figure 2.2.

The known parameters and unknown parameters are shown in Table 2.1.

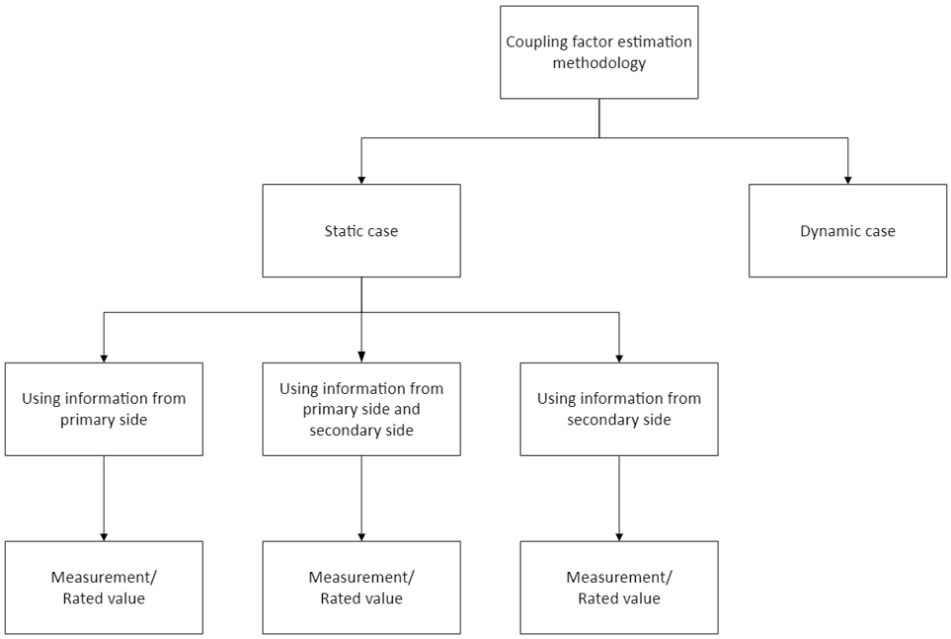

Figure 2.1: Existing methodology

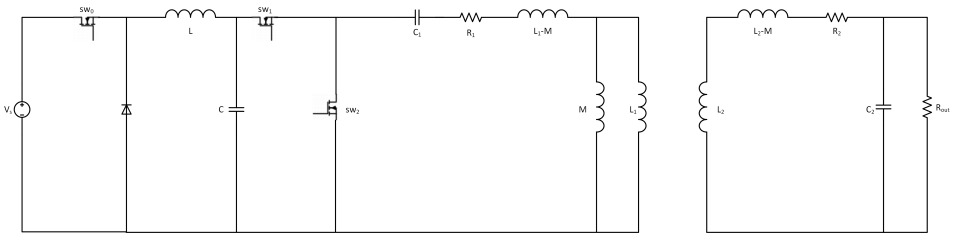

Figure 2.2: Circuit topology of [20]

The input voltage can be changed by using switch sw0, as a dc-dc converter. The operating frequency can be changed by switch 1 and switch 2, as a resonant inverter. The circuit will be operated in three different frequency, fa, fb and fc. fb and fc are multiples of fundamental frequency fa.

The flow chart of this methodology is shown in Figure 2.3.

For each frequency case, v_{in} and i_{in} will be sampled first. After applying Goertzel algorithm, the voltage, current and phase of these three frequencies can be obtained. Then, the capacitance of the secondary side can be calculated by the frequency a and b component. Similarly, the capacitance of the secondary side by frequency a and c component can also be obtained. After that, the deviation between these two values can be calculated, and the minimum deviation is the capacitance of the secondary side.

Mutual inductance can be obtained in a similar way when the capacitance of the secondary side is known.

Table 2.1: Known and unknown parameters of [20]

Known parameters	Unknown parameters
Self inductance, Resistance, Capacitance of the primary side, Frequency, Phase	Capacitance of the secondary side, Mutual inductance

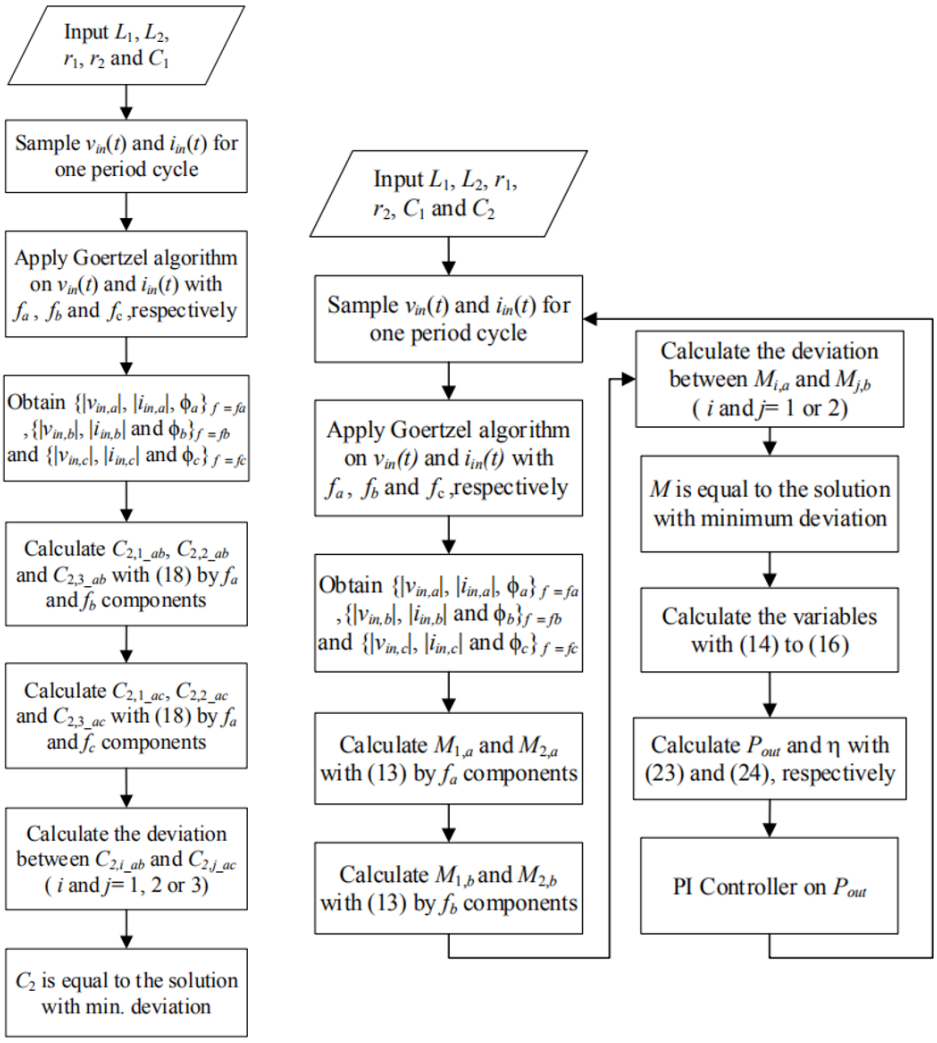

Figure 2.3: Flow chart of [20]

[21] proposed a methodology that uses the voltage and current of the secondary side to obtain the mutual inductance and voltage of the primary side. The circuit topology is shown in Figure 2.4.

A half active rectifier is applied on the secondary side and so that the system will work in rectification mode or short mode as the Figure 2.5 shown.

The known parameters and unknown parameters are shown in the Table 2.2.

First, two sets of electrical parameters of two different operation modes are obtained. Then equations between known parameters and unknown parameters can be built.

$$I_2 \simeq \frac{\omega_0 L_m V_{11} - R_1 V_{21}}{R_1 R_2 + (\omega_0 L_m)^2} = \frac{2\sqrt{2}}{\pi} \frac{\omega_0 L_m V_1 - R_1 V_2}{R_1 R_2 + (\omega_0 L_m)^2} \tag{2.2}$$

Table 2.2: Known and unknown parameters of [21]

Known parameters	Unknown parameters
The current and voltage of the secondary side, Frequency, Resistance	Mutual inductance, The voltage of the primary side

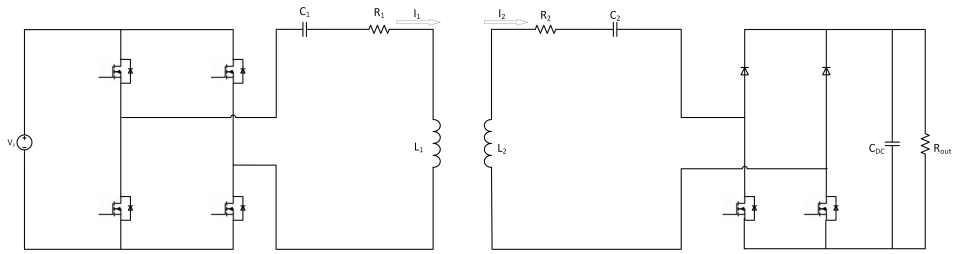

Figure 2.4: Circuit topology of [21]

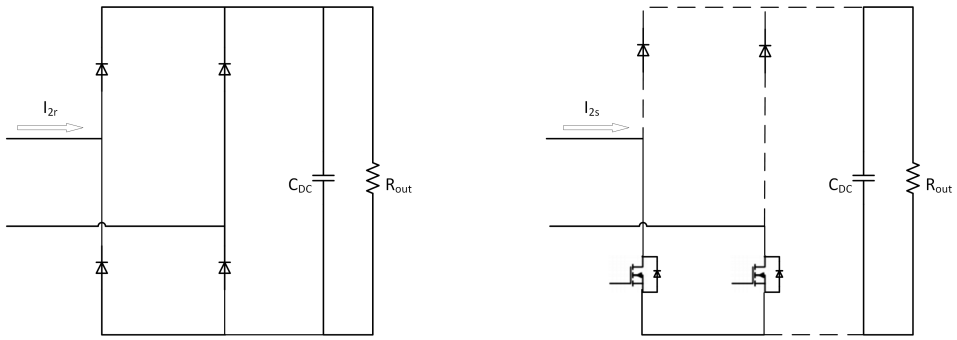

(a) Rectification mode (b) Short mode

Figure 2.5: Circuit topology of [21]

$$\omega_0 = \frac{1}{\sqrt{L_1 C_1}} = \frac{1}{\sqrt{L_2 C_2}} \tag{2.3}$$

$$\omega_0 L_m V_{11} - I_2 (\omega_0 L_m)^2 = R_1 (V_{21} + R_2 I_2) \tag{2.4}$$

Where L_1, L_2, C_1 and C_2 are the inductance and capacitance of the primary side and the secondary side. R_1 and R_2 are the resistance of the primary side and the secondary side. ω_0 is the resonant frequency, L_m is the mutual inductance, V_{11} and V_{21} are the RMS values of the fundamental primary and secondary voltages, I_{11} and I_2 are the RMS values of the fundamental primary and secondary current.

The equation then can be derived to

$$\begin{aligned} &x_1 - I_2 x_2 = R_1 (V_{21} + R_2 I_2) \\ &x = \begin{bmatrix} x_1 & x_2 \end{bmatrix}^T := \begin{bmatrix} \omega_0 L_m V_{11} & (\omega_0 L_m)^2 \end{bmatrix}^T \end{aligned} \tag{2.5}$$

$$\begin{aligned} &\hat{x} = \begin{bmatrix} \hat{x}_1 & \hat{x}_2 \end{bmatrix}^T = A^{-1} b \\ &A := \begin{bmatrix} 1 & -I_{2r} \\ 1 & -I_{2s} \end{bmatrix}, b := \begin{bmatrix} R_1 (V_{21r} + R_2 I_{2r}) \\ R_1 (V_{21s} + R_2 I_{2s}) \end{bmatrix} \end{aligned} \tag{2.6}$$

Therefore, the primary side information can be calculated by solving these equations.

$$\begin{aligned} &V_{21r} = \frac{2\sqrt{2}}{\pi} V_{2r} = \frac{2\sqrt{2}}{\pi} \left(V_{dc} + 2V_f\right) \\ &V_{21s} = \frac{2\sqrt{2}}{\pi} V_{2s} = 0 \\ &\hat{L}_m = \frac{1}{\omega_0} \sqrt{\hat{x}_2} \\ &\hat{V}_1 = \frac{\pi}{2\sqrt{2}} \hat{V}_{11} = \frac{\pi}{2\sqrt{2}} \frac{\hat{x}_1}{\omega_0 \hat{L}_m} \end{aligned} \tag{2.7}$$

Table 2.3: Known and unknown parameters of [7]

Known parameters	Unknown parameters
Radius, Space, Turns, Loop current, Frequency	Mutual inductance

[7] introduced a unique methodology that uses the geometry of the coil of transmitter and receiver to calculate the information of the secondary side. The system and coils are shown in Figure 2.6.

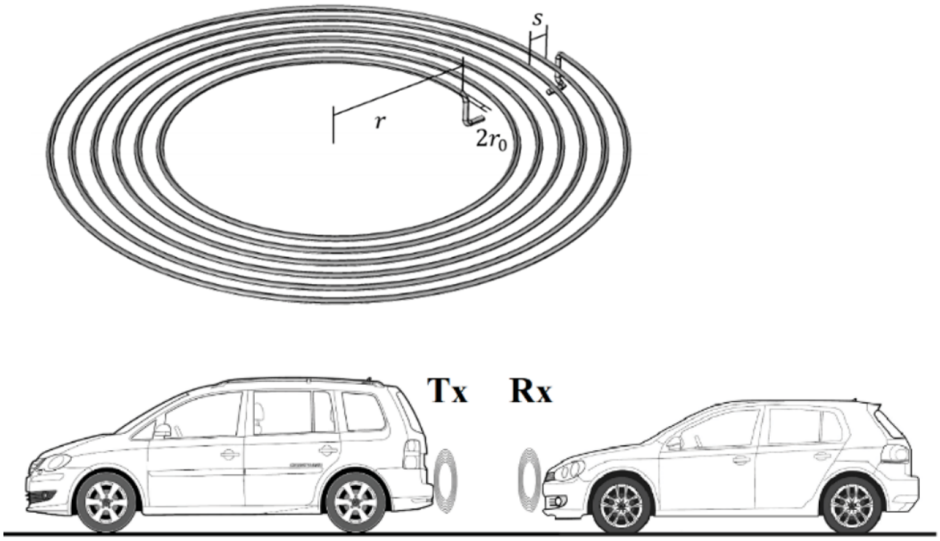

Figure 2.6: System and coils topology of [7]

The known parameters and unknown parameters are shown in the Table 2.3.

First, the relationship between radius and turns can be calculated by mathematical derivation.

$$r_i = r_1 + \frac{s}{2} + (i-1)s$$

$i = 1, 2, 3, \ldots N$ - Total number of turns

Then the equation of magnetic vector potential in any point on the open loop can be built according to Ampere's law.

$$A_\varphi = \frac{\mu_0 I_1}{4\pi} 2 \oint_0^\pi \frac{r_1 \cos\varphi d\varphi}{\sqrt{r_1^2 + r_2^2 - 2r_1 r_2 \cos\varphi + d^2}} \tag{2.8}$$

Parameter k is assumed as the equation 2.9.

$$k = 2\sqrt{\frac{r_1 r_2}{(r_1 + r_2)^2 + d^2}} \tag{2.9}$$

Based on the mathematical analysis, the expression of self inductance and mutual inductance can be obtained. K(k) and E(k) are the complete elliptic integrals of the first and the second kind.

$$\begin{aligned} M &= \frac{2\mu_0\sqrt{r_1 r_2}}{k}\left[\left(1 - \frac{k^2}{2}\right)K(k) - E(k)\right] \\ M &= \sum_i^{N_1}\sum_j^{N_2} \frac{2\mu_0\sqrt{r_i r_j}}{k}\left[\left(1 - \frac{k^2}{2}\right)K(k) - E(k)\right] \end{aligned} \tag{2.10}$$

In [22] a derivation for the equations for estimating the coupling factor in single receiver WPT systems and multiple receivers WPT systems by using the information from only the transmitting side or the receiving side has been given. The equation with impedance, operating frequency and mutual inductance can be derived by the equivalent circuit in Figure 2.7 and Figure 2.8.

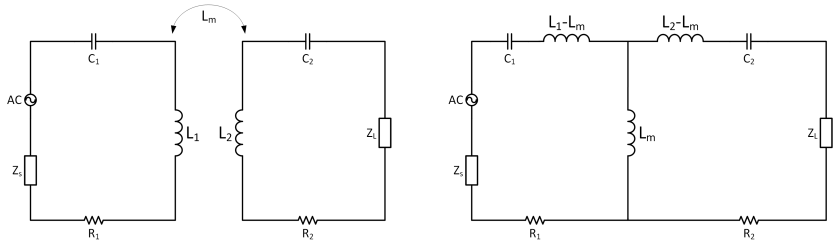

Figure 2.7: Circuit topology of a single receiver of [22]

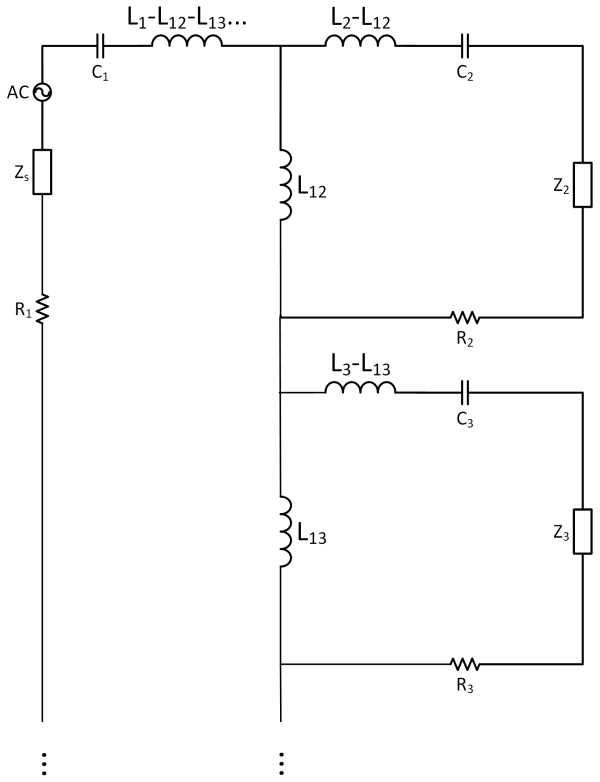

Figure 2.8: Circuit topology of multiple receivers of [22]

The known parameters and unknown parameters are shown in Table 2.4.

$$L_m = \frac{1}{\omega}\sqrt{\frac{[\mathrm{Re}\{Z_{\mathrm{in}}\} - R_1]\left[(Z_L + R_2)^2 + Z_{A2}^2\right]}{Z_L + R_2}} \tag{2.11}$$

For multiple receivers, based on the information of receiving side, the equation 2.12 and 2.13 can be build.

$$\begin{bmatrix} Z_{\mathrm{in}\,(1)} \\ Z_{\mathrm{in}\,(2)} \\ \vdots \end{bmatrix} = \begin{bmatrix} P_1 \\ P_2 \\ \vdots \end{bmatrix} + \begin{bmatrix} Q_{11} & Q_{12} & \cdots \\ Q_{21} & \ddots & \vdots \\ \vdots & \cdots & Q_{mm} \end{bmatrix} \begin{bmatrix} L_{12}^2 \\ L_{13}^2 \\ \vdots \end{bmatrix} \tag{2.12}$$

Table 2.4: Known and unknown parameters of [22]

Known parameters	Unknown parameters
The current, voltage of primary side, Frequency, Self inductance of primary side and secondary side, Capacitance of both two sides, Load, Resistance	Mutual inductance

$$\begin{aligned} P_v &= R_1 + j\omega_v L_1 + \frac{1}{j\omega_v C_1} \\ Q_{uv} &= \frac{\omega^2}{Z_u + R_u + j\omega_j L_u + \frac{1}{j\omega_v C_u}} \end{aligned} \tag{2.13}$$

For a single receiver, based on the information of receiving side, the inductance is shown in equation 2.14.

$$L_m = \frac{1}{2\omega}\left[\frac{V_1}{V_2}Z_2 \pm \sqrt{\left(\frac{V_1}{V_2}Z_2\right)^2 + 4R_1\left(R_2 + Z_2\right)}\right] \tag{2.14}$$

For multiple receivers, based on the information of receiving side, the inductance is shown in equation 2.15.

$$L_{12} = \frac{V_1}{\omega}\frac{Z_{2a}V_{2b}\left(R_2 + Z_{2b}\right) - Z_{2b}V_{2a}\left(R_2 + Z_{2a}\right)}{V_{2a}V_{2b}\left(Z_{2b} - Z_{2a}\right)} \tag{2.15}$$

Therefore, the coupling coefficient can be derived. The result is verified by an experimental system.

Based on a series-series-type WPT system,[19] added an extra capacitor in the system, so that the system can work in two operation modes. Based on the two different operation modes, the respective mathematical model will be established and analyzed. The capacitance switching schematic is shown in Figure 2.9.

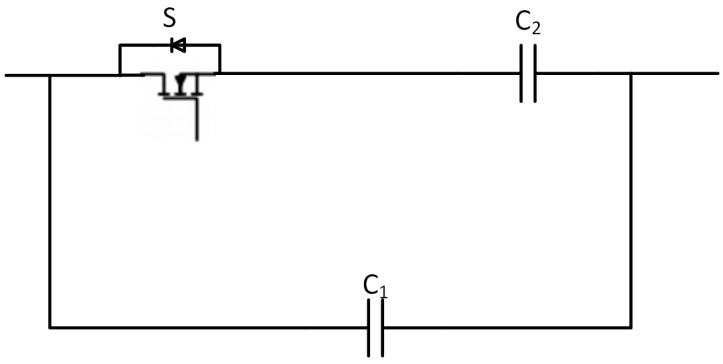

Figure 2.9: The schematic of capacitance switching [19]

The known parameters and unknown parameters are shown in Table 2.5.

The working mode can be changed by opening or closing the switch. In working mode 1, the switch is off and the system is designed to be in full resonance. There is only C1 in the capacitance switching part. In working mode 2, the switch is on and both C1 and C2 are placed in the circuit. The operating frequency is adjusted by detecting the current zero crossings. There are two sets of electrical parameters of the system based on two operating modes.

Table 2.5: Known and unknown parameters of [19]

Known parameters	Unkonwn parameters
Current, voltage of primary side, resonant frequency, self inductance, capacitance, resistance	Mutual inductance, load

Based on the basic theory of reflected impedance, the equation of impedance can be derived as equation 2.16.

$$\begin{aligned} Z_s &= j\omega L_s + \frac{1}{j\omega C_s} + j\,\mathrm{Im}\,Z_L + \mathrm{Re}\,Z_L + R_s \\ Z_r &= \omega^2 M^2 / Z_s = \mathrm{Re}\,Z_r + j\,\mathrm{Im}\,Z_r \end{aligned} \tag{2.16}$$

When the system is operated in mode 1(there is only C_1 in the circuit), the resonant frequency of this circuit can be written as equation 2.17:

$$\frac{1}{\omega_{\text{ref}}^2} = L_p C_p = L_s C_s \tag{2.17}$$

When the system is operated in mode 1(there are both C_1 and C_2 in the circuit), the resonant frequency of this circuit can be written as equation 2.18:

$$\frac{1}{\omega_{\text{ref}}^2} = L_p \cdot (C_1 + C_2) \tag{2.18}$$

The imaginary part of the reflected impedance of the primary side is zero when the system is under the full primary resonance.

$$\omega L_p - \frac{1}{\omega C_p} + \mathrm{Im}\,Z_r = 0 \tag{2.19}$$

The real part of the reflected impedance of the primary side can be obtained by the formula 2.20.

$$I_p = \frac{U_p}{\mathrm{Re}\,Z_r + R_p} \tag{2.20}$$

According to the equation of the impedance and the system's electrical parameters, the equation of the inductance and mutual inductance can be established.

$$L = \frac{\alpha \cdot \beta + \gamma \cdot \lambda}{\omega_1 \cdot \alpha - \omega_2 \cdot \gamma} \tag{2.21}$$

$$\begin{aligned} \alpha &= \mathrm{Im}\,Z_{r1} \cdot \left(0.9E_{\mathrm{DC}} - I_{p2}R_p\right) \cdot I_{p1} \\ \beta &= \omega_2 L_s - \frac{1}{\omega_2 C_s} \\ \gamma &= \mathrm{Im}\,Z_{r2} \cdot \left(0.9E_{\mathrm{DC}} - I_{p1}R_p\right) \cdot I_{p2} \\ \lambda &= \omega_1 L_s - \frac{1}{\omega_1 C_s} \end{aligned} \tag{2.22}$$

$$M = \sqrt{\frac{\mathrm{Im}\,Z_{r2} \cdot \left[\mathrm{Re}\,Z_s^2 + \left(\frac{1}{\omega_2 C_s} - \omega_2 L_s - \omega_2 L\right)^2\right]}{\omega_2^2 \left(\frac{1}{\omega_2 C_s} - \omega_2 L_s - \omega_2 L\right)}} \tag{2.23}$$

Therefore, the coupling factor can be calculated.

Except for static wireless charging, dynamic wireless charging is also needed. Unlike the static WPT system, the coupling factor of a dynamic WPT system will change drastically when the primary side or the secondary side moves. Estimating the change of coupling factor is necessary to monitor

the system. Literature [23] proposed a maximum WPT system efficiency tracking method based on dynamic WPT system coupling factor estimation. The schematic of the main circuit of the dynamic WPT system is shown in Figure 2.10.

The output voltage can be controlled by changing the duty cycle d1 of the primary side buck-boost

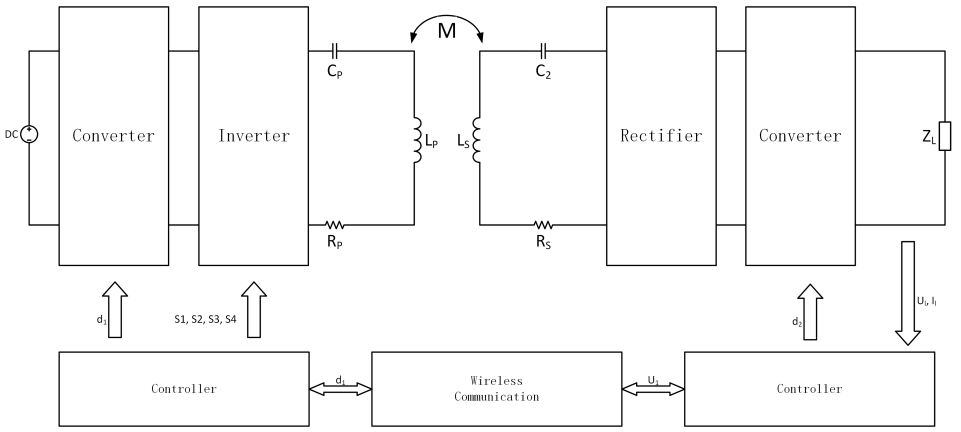

Figure 2.10: Circuit topology of [23]

converter. The load can be controlled by changing the duty cycle d2 of the secondary-side buck-boost converter.

First, similar to the estimation of the coupling factor of a static WPT system, the initial coupling coefficient can be estimated based on the circuit analysis. The relationship between the coupling factor and the duty cycle is obtained according to the circuit analysis.

$$Z_s = \frac{8}{\pi^2}\left(\frac{1-d_2}{d_2}\right)^2 R_l + R_s \tag{2.24}$$

$$U_s = U_{\text{in}}\frac{2\sqrt{2}d_1}{\pi\,(1-d_1)} \tag{2.25}$$

$$I_p = \frac{U_s}{R_p + Z_{\text{ref}}} \tag{2.26}$$

$$\alpha = \frac{\sqrt{2}\pi R_{r-in} d_2}{4\,(R_{r-in}+R_s)\,(1-d_2)} \tag{2.27}$$

$$k = \frac{\alpha U_s Z_s \pm \sqrt{(\alpha U_s Z_s)^2 - 4R_p U_l^2 Z_s}}{2\omega U_l \sqrt{L_p L_s}} \tag{2.28}$$

If there is a difference between the required output voltage and the real output voltage, the duty cycle d1 will automatically change. The relationship of the previous coupling factor, the latest coupling factor and the duty cycle d1 can be derived by mathematical derivation.

$$\begin{aligned}
&\xi = {U_{l-\,\text{req}}}^2 R_p\left({d_2}^2\left(2\pi^4 R_s + 16\pi^2 R_l\right) - 32\pi^2 R_l d_2 + 16\pi^2 R_l\right),\\
&\psi = U_{l-\text{req}}^2 R_p\left(d_2^2\left(-\pi^4 R_s - 8\pi^2 R_l\right) + 16\pi^2 R_l d_2 - 8\pi^2 R_l\right),\\
&\delta = {U_{l-\text{req}}}^2 R_p\left(d_2^2\left(-\pi^4 R_s - 8\pi^2 R_l\right) + 16\pi^2 R_l d_2 - 8\pi^2 R_l\right)\\
&\quad + U_s^2 R_l^2\left(16d_2^2 - 32d_2 + 16\right),\\
&\beta = \frac{-1}{U_{l-\text{req}}\pi^2\omega d_2},\quad \gamma = 4U_s R_l\,(1-d_2)\,.
\end{aligned} \tag{2.29}$$

$$\frac{\left[\left(k_p + \Delta k\right) - k_p\right]}{\left[\left(d_{1p} + \Delta d_1\right) - d_{1p}\right]} = \left.\frac{\partial f\,(d_1)}{\partial d_1}\right|_{d_1 = d_{1p}} \tag{2.30}$$

$$\frac{\Delta k}{\Delta d_1} = \left.\frac{\partial f(d_1)}{\partial d_1}\right|_{d_1=d_{1p}} \tag{2.31}$$

$$\mathrm{k}_l = k_p + \Delta d_1 \left.\frac{\partial f(\mathrm{d}_1)}{\partial d_1}\right|_{d_1=d_{1p}} \tag{2.32}$$

The flow chart is shown in Figrue 2.11.

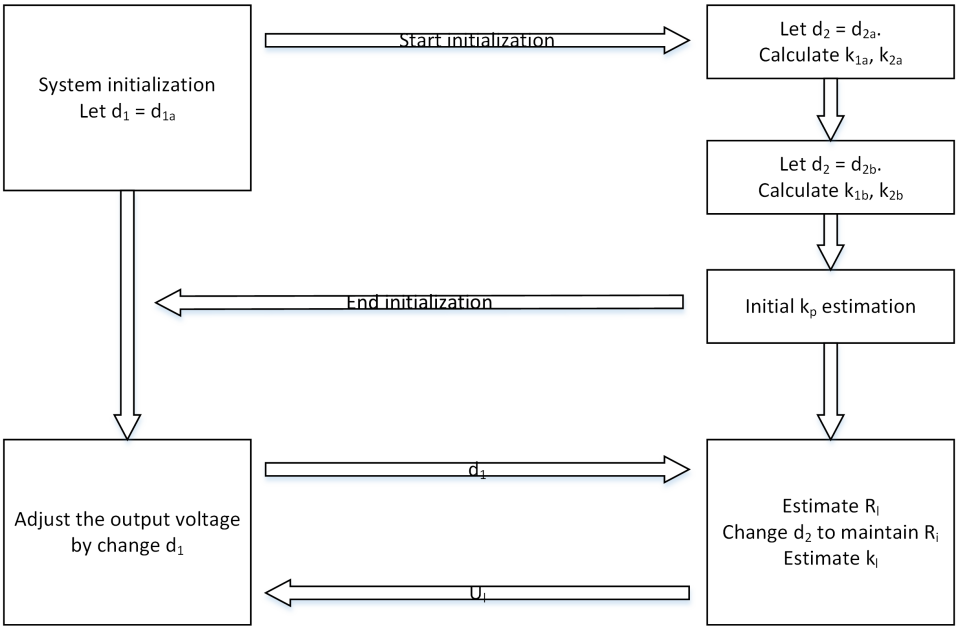

Figure 2.11: Flow chart of [23]

Therefore, the dynamic coupling factor estimation can be implemented.

2.3. Summary

The summary table of these methodologies is shown in Table 2.6.

Table 2.6: Summary table of the common methodologies

Method	Advantage	Disadvantage
Online estimation based on the primary side information	Only require information of primary side.	Complex calculation.
Estimation based on the secondary information	Only require information of the secondary side.	External circuit is required in the secondary side.
Estimation based on geometry properties	Do not require many electrical parameters.	Ignore the misalignment.
Estimation based on circuit analysis of the primary side or the secondary side information	Clear and simple.	Information of load is required.
Estimation based on switching capacitors	Clear and simple. Information of load is not required.	An external circuit is required on the primary side.
Dynamic estimation based on changing duty cycle	Estimation of the dynamic wireless charging.	Complex control and calculation.

The method 'online estimation based on primary side information' let the circuit operate in three different frequencies and use three sets of parameters to obtain the information of the secondary side and mutual inductance. The advantage is that it only uses the information of the primary side. However, the calculation is too complex.
The method 'estimation based on secondary information' let the circuit operate in two different modes. The mutual inductance can be calculated based on these two sets of parameters. It only uses information of the primary side but it will add an external circuit on the secondary side.
The method 'estimation based on geometry properties' provides an innovative method that uses the geometry of the coil to obtain the mutual inductance. It doesn't need many electrical parameters but it ignores the misalignment of coils.
The method 'estimation based on circuit analysis of primary side or receiving side information ' obtain the mutual inductance based on the parameters from both the primary side and the secondary side. However, it needs the information of the load.
The method 'estimation based on switching capacitors' makes the circuit work under two different capacitance of the primary side. Then the mutual inductance and load can be identified. A external circuit on the primary side is needed, but it is easy to implement.
The method 'dynamic estimation based on changing duty cycle' obtain the mutual inductance of dynamic wireless charging by adjusting the duty cycle of the buck-boost converter. However, the control of the system is complex and the calculation of mutual inductance is complex. In summary, the methodology 'estimation based on switching capacitors' has a better performance compared with other methodologies. Therefore, this thesis will focus on this methodology. The simulation will be implemented in the next section. Besides, in order to compare the accuracy of this methodology, the simulation of another method of 'estimation from the information of primary side or receiving side' will also be implemented.

3

Simulation based study of parameter identification

In this section, the simulation of the selected method will be implemented. The methodology structure of the literature [19] is shown in Figure 3.1.

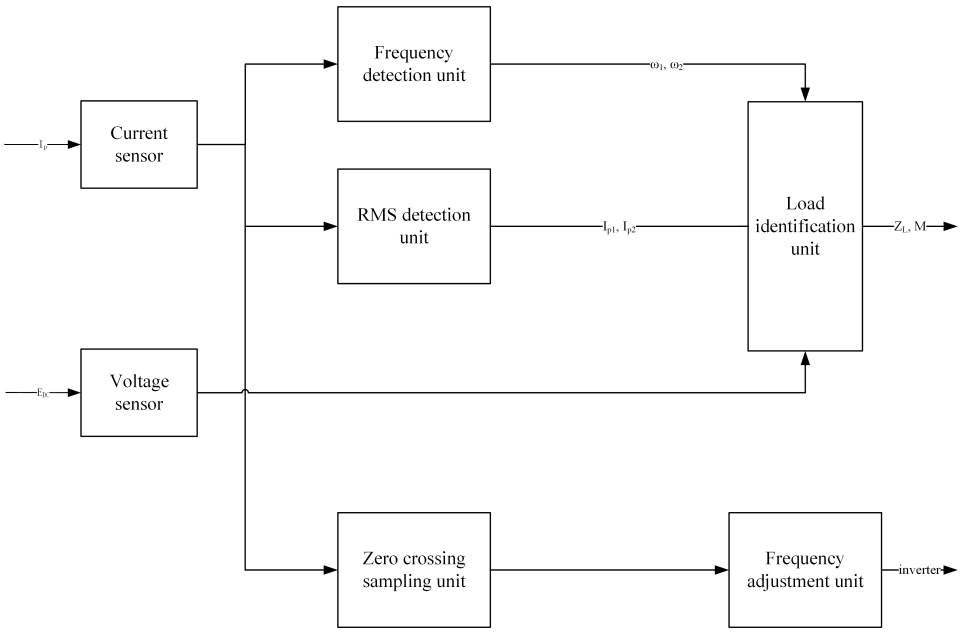

Figure 3.1: Flow chart of [19]

First, the information of the current and voltage from the primary side can be obtained by the current sensor and voltage sensor. Then the information of current will be sent to three different units. The first is the frequency detection unit. After receiving the current information, the two different frequencies can be obtained. The second is the RMS detection unit. The RMS value of two different currents will be calculated after receiving the current information. Both frequency information and RMS information of the current will be sent to the identification unit. Besides, the information of voltage will also be sent to the identification unit. Then the load information and coupling factor can be obtained. The last unit for the current information is the zero crossing unit. The inverter operating frequency is adjusted by detecting the current zero crossings to make the system work under the primary resonant state.

Therefore, the system can be separated into six unit. Frequency detection unit, RMS detection unit, zero crossing unit, frequency adjustment unit and load identification unit and mutual inductance

identification unit.

3.1. Assumption

There are some assumptions of simulation.
First, when the primary side is resonant, the primary side impedance, including the reflected impedance of the secondary, is zero. Besides, the circuit is always operating at the resonant frequency.
Second, when the system works in soft-switching mode, the switching loss can be ignored. Therefore, only the copper loss is considered in the system modeling.
Third, the load does not change much under normal operating condition.

3.2. Circuit topology and operation principle

The circuit outline is shown in Figure 3.2.

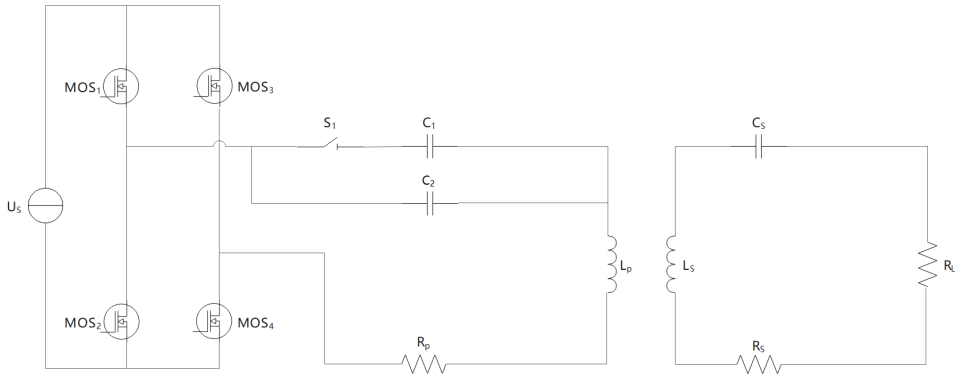

Figure 3.2: Circuit topology

3.2.1. Basic topology

For wireless power transfer systems, as section 3 introduced, it required compensation networks in the primary side or the secondary side to improve the power factor and transfer efficiency. In order to make the capacitance independent of load and coupling factor, this methodology applied series to series compensation network.

On the primary side, the voltage source is a DC voltage source. The full-bridge inverter consists of four MOSFETs. All of these MOSFETs should work in zero current switching mode. Through this inverter network, the DC voltage will be converted to the alternating square wave voltage. The resonant network of the primary side consists of controlled capacitance and an inductor. The alternating current is generated from this resonant network. Therefore, an alternating magnetic field will be generated on the primary side's winding.

On the secondary side, the secondary side's winding will receive the power from the alternating magnetic field of the primary side through magnetic field coupling. The resonant network in the secondary side is consist of a capacitance and an inductor. The load is powered by the secondary side through this resonant network.

3.2.2. Equivalent primary side voltage

On the primary side, the capacitance and the inductor can be regarded as a low pass filter. This low pass filter can efficiently reduce the high frequency harmonic voltage and high frequency harmonic current. Therefore, for the frequency adjusting unit, only the fundamental resonant frequency needs

to be considered. When the full-bridge inverter works in soft switching mode, the RMS value of the primary side voltage can be expressed as:

$$U_p = \frac{4E_{\mathrm{DC}}}{\sqrt{2}\pi} = 0.9E_{\mathrm{DC}} \tag{3.1}$$

3.2.3. Equivalent load

The load of the secondary side can be the battery of the vehicle or the battery of other electronic products. To simplify, the load is equivalent to pure resistance.

3.2.4. Two different modes of controlled capacitance in the primary side

There are two capacitances in the primary side circuit. For capacitance 1, it is connected to the circuit directly. For capacitance 2, a controllable switch is applied to connect it to the circuit. Through this controllable switch, the wireless power transfer system can work in two different modes with two different primary side capacitance. For the circuit parameter designing, the value of capacitance 2 is required to make the system have an observable change, including the resonant frequency and the current. However, the value of capacitance should not be too large otherwise it will cause high stress on the circuit component.

3.2.5. Circuit analysis

In order to study this estimation method, the circuit should be analyzed theoretically.
According to Kirchhoff's law,

$$\begin{aligned} U_s &= \left(R_p + j\omega L_p + \frac{1}{jC_p}\right) I_p - j\omega M I_s \\ 0 &= -j\omega M I_p + \left(R_s + R_L + j\omega L_s + \frac{1}{j\omega C_s}\right) I_s \end{aligned} \tag{3.2}$$

According to the equation, the relationship between I_P and I_S can be obtained.

$$I_s = \frac{j\omega M}{j\omega L_s + R_s + R_L} I_p \tag{3.3}$$

To combine the equation 3.2 and equation 3.3, I_P can be expressed as

$$I_p = \frac{U_p}{\left(j\omega L_p + R_p\right) + \frac{(\omega M)^2}{j\omega L_s + R_s + R_L}} \tag{3.4}$$

Let

$$\begin{aligned} Z_p &= R_p + j\omega L_p + \frac{1}{j\omega C_p} \\ Z_s &= R_s + R_L + j\omega L_s + \frac{1}{j\omega C_s} \end{aligned} \tag{3.5}$$

The input impedance of the primary side is

$$Z_{in} = \frac{U_p}{I_p} = Z_p + \frac{(\omega M)^2}{Z_s} \tag{3.6}$$

Therefore, the reflected impedance Z_r can be expressed as

$$Z_r = \frac{(\omega M)^2}{Z_s} = ReZr + ImZr \tag{3.7}$$

The equation of the real part and the imaginary part of the reflected impedance can be obtained

$$\begin{aligned} \mathrm{Re}\, Z_r &= \frac{\omega^2 M^2 \left(R_s + \mathrm{Re}\, Z_L\right)}{\left(R_s + \mathrm{Re}\, Z_L\right)^2 + \left(1/\omega C_s - \omega L_s - \mathrm{Im}\, Z_L\right)^2} \\ \mathrm{Im}\, Z_r &= \frac{\omega^2 M^2 \left(1/\omega C_s - \omega L_s - \mathrm{Im}\, Z_L\right)}{\left(R_s + \mathrm{Re}\, Z_L\right)^2 + \left(1/\omega C_s - \omega L_s - \mathrm{Im}\, Z_L\right)^2} \end{aligned} \tag{3.8}$$

According to the subsection 1.1, the energy will be transferred from the primary side to the secondary side through the primary side winding. The transferred energy from the primary side to the secondary side will be consumed by the real part of the reflecting impedance from the secondary side. The imaginary part of the reflecting impedance and the primary side winding are used to store and release energy. Therefore, to operate the system in full resonance state is necessary to improve the magnetic factor and maximize the power transfer. If there is no load on the secondary side, both the primary side and the secondary side will operate in natural resonant frequency.

$$\frac{1}{\omega_{\mathrm{ref}}^2} = L_p C_p = L_s C_s \tag{3.9}$$

The imaginary part of the primary side will be zero if the primary side is under resonant. The imaginary part of the primary side consists of ωL_p, $\frac{1}{\omega C_p}$ and the imaginary part of the reflected impedance of the secondary side. Therefore, the relationship below can be built.

$$\omega L_p - \frac{1}{\omega C_p} + \operatorname{Im} Z_r = 0 \tag{3.10}$$

When the system is operated in full resonant frequency, the real part of the reflected impedance can be calculated as

$$I_p = \frac{U_p}{\operatorname{Re} Z_r + R_p} \tag{3.11}$$

By applying the capacitance switch S, the system will be operated in two different modes with two different primary compensation capacitances.
There is only primary capacitance C_1 in the primary circuit when switch S is off. The system will be adjusted to operate in primary resonant frequency f_1 by applying the zero crossing unit to detect the current zero crossing on the primary side. Another primary compensation capacitance C_2 will be connected to the primary circuit when the switching S is on. Similarly, the system operating frequency will be adjusted to primary resonant frequency f_2 by zero crossing unit. The mutual inductance detection and load detection will be implemented based on two different sets of electrical parameters. The details of two different operation modes will be analyzed.

For operation mode 1: The switch S is off and only primary compensation capacitance C_1 is connected to the primary circuit. The primary side current I_{p1} can be represented as

$$I_{p1} = \frac{U_p}{\operatorname{Re} Z_{r1} + R_p} \tag{3.12}$$

The reflected impedance of the secondary side Z_{r1} can be represented as

$$Z_{r1} = \omega_1^2 M^2 / Z_s \tag{3.13}$$

For operation mode 2: The switch S is on and both primary compensation capacitance C_1 and C_2 are connected to the primary circuit. The primary side current I_{p2} can be represented as

$$I_{p2} = \frac{U_p}{\operatorname{Re} Z_{r2} + R_p} \tag{3.14}$$

The reflected impedance of the secondary side Z_{r2} can be represented as

$$Z_{r2} = \omega_1^2 M^2 / Z_s \tag{3.15}$$

According to the formula 3.10, when the circuit is operated in full resonant frequency, the imaginary part of the reflected impedance can be calculated as

$$\begin{aligned} \operatorname{Im} Z_{r1} &= \frac{1}{\omega_1 C_1} - \omega_1 L_p \\ \operatorname{Im} Z_{r2} &= \frac{1}{\omega_2 (C_1 + C_2)} - \omega_2 L_p \end{aligned} \tag{3.16}$$

Table 3.1: Symbol of system parameters

Symbol	Definition	Value
C_1	Primary side compensation capacitance	Known
C_2	Primary side compensation capacitance	Known
L_p	Primary side compensation inductance	Known
R_p	Primary side resistance	Known
C_s	Secondary side compensation capacitance	Known
L_s	Secondary side compensation inductance	Known
R_s	Secondary side resistance	Known
E_{DC}	Primary side DC voltage	Measured value
I_{p1}	Primary side current when the circuit is operated in mode 1	Measured value
I_{p2}	Primary side current when the circuit is operated in mode 2	Measured value
f_1	Primary side frequency when the circuit is operated in mode 1	Measured value
f_2	Primary side frequency when the circuit is operated in mode 2	Measured value

Table 3.2: Values of system parameters

Parameters	Values
Primary side DC voltage E_{DC}	10 V
Primary side compensation inductance L_p	362 μH
Secondary side compensation inductance L_s	155 μH
Primary side compensation capacitance C_1	27.7 nF
Secondary side compensation capacitance C_s	65.9 nF
Primary side resistance R_p	1.3 Ω
Secondary side resistance R_s	0.32 Ω

Therefore, the load can be calculated as

$$R_L = \frac{\left(0.9E_{\mathrm{DC}} - I_{p2}R_p\right) \cdot \left(\frac{1}{\omega_2 C_s} - \omega_2 L_s - \omega_2 L\right)}{\mathrm{Im}\, Z_{r2} \cdot I_{p2}} - R_s \tag{3.17}$$

Besides, the mutual inductance can be calculated as

$$M = \sqrt{\frac{\mathrm{Im}\, Z_{r2}\left[ReZ_s^2 + \left(\frac{1}{\omega_2 C_s} - \omega_2 L_s\right)^2\right]}{\omega_2^2\left(\frac{1}{\omega_2 C_s} - \omega_2 L_s\right)}} \tag{3.18}$$

The parameters of these formulas are shown in the table below.

3.3. Simulation model implementation

The circuit typology in Simulink is shown in Figure 3.3.
The signal input A and B is the output of the zero crossing unit. These two controlled signals will make the circuit operate under full resonant. The details of the zero crossing unit will be shown later.
The parameter of the circuit is shown in Figure 3.1 and 3.2.

3.3.1. Zero crossing implementation

In order to make the system operate in the primary resonant state, the full-bridge inverter working frequency should be adjusted by detecting the primary side current zero crossings. Therefore, a zero crossing detection unit is required.
The zero crossing implementation is shown in Figrue 3.4. The signal of the primary side current will enter this unit and be compared with zero. For the upper comparator, if the input is larger than zero, the output will be high. Otherwise, the upper output will be low. For the lower comparator, if the input is

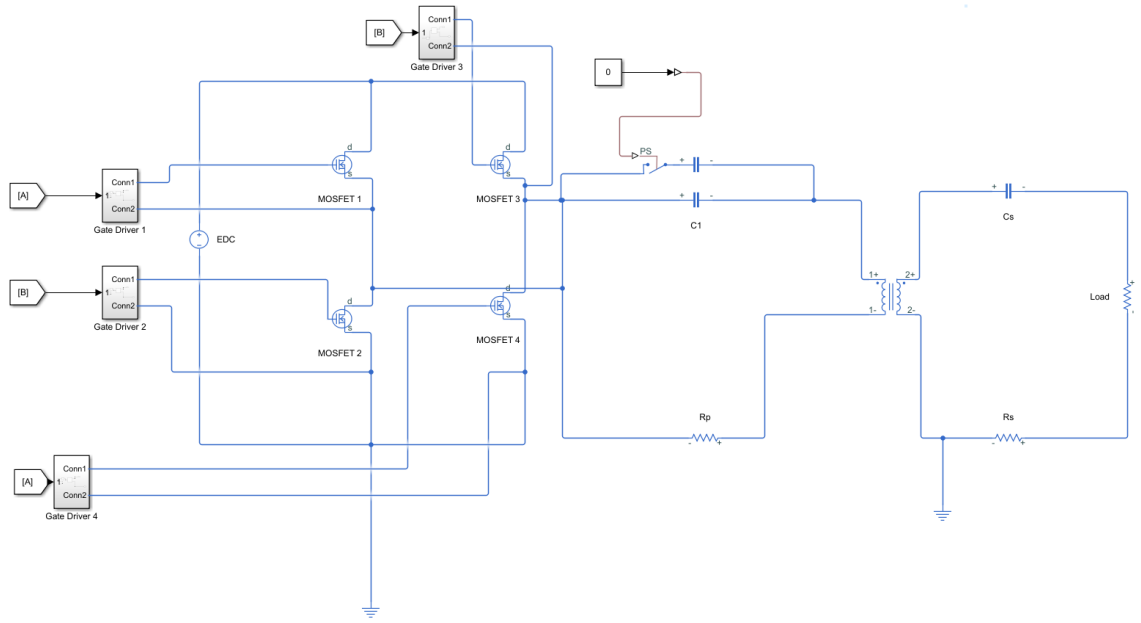

Figure 3.3: Circuit typologies in Simulink

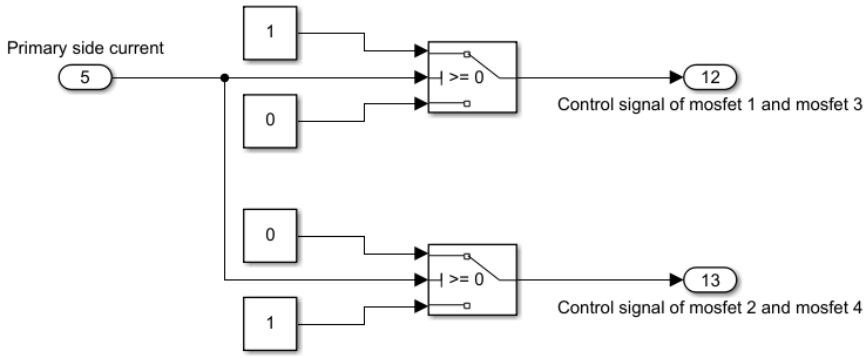

Figure 3.4: Zero crossing unit

larger than zero, the output will be low. Otherwise, the upper output will be high. This unit will generate two opposite control signals to the MOSFET of the full-bridge converter. The frequency of this control signal will be the primary side resonant frequency.
The input signal and output signal in two different operation modes are shown in the figure below.
According to these waveforms in Figure 3.5 and 3.6, two complementary square wave signals are generated based on the input signal. When the value of the input signal is larger than 0, a square wave output signal will be set as 1 and another square wave output signal will be set as 0.
Therefore, the system can be operated in the primary side resonant frequency by applying this zero crossing unit in the full bridge inverter.

3.3.2. PLL implementation and RMS implementation

The frequency of the input signal is required in RMS calculation. Therefore, a frequency detection unit is required in this system. Phase locked loop is a commonly used unit to detect the phase and frequency of the signal. Literature[24] proposed a Park PLL schematic. The block consists of a PI controller, two filters, a Park transformation unit and an inverse Park transformation unit. The schematic is shown In Figure 3.7.

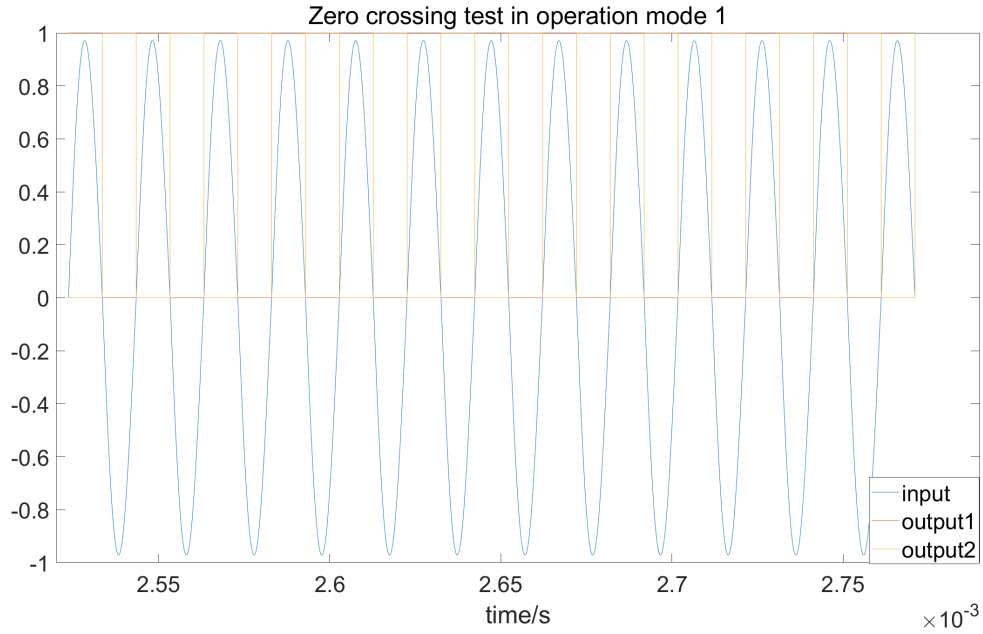

Figure 3.5: Input and output of zero crossing in operation mode 1

Assume the input signal ei is a purely sinusoidal signal in the form $Vcos\theta$. Where V is the amplitude of the input signal, θ is the signal angle and $\hat{\theta}$ is the estimated signal angle. $\hat{\omega}$ is the estimated angular frequency of input signal.

The components v_d and V_q are obtained by Park transformation. Besides, the component V_β is obtained by inverse Park transformation unit.

The Park transformation matrix is shown in equation 3.19.

$$\begin{bmatrix} v_d \\ v_q \end{bmatrix} = \begin{bmatrix} \sin\hat{\theta} & \cos\hat{\theta} \\ \cos\hat{\theta} & -\sin\hat{\theta} \end{bmatrix} \begin{bmatrix} v_\alpha \\ v_\beta \end{bmatrix} \tag{3.19}$$

The Park inverse transformation matrix is shown in equation 3.20.

$$\begin{bmatrix} v'_\alpha \\ v_\beta \end{bmatrix} = \begin{bmatrix} \sin\hat{\theta} & \cos\hat{\theta} \\ \cos\hat{\theta} & -\sin\hat{\theta} \end{bmatrix} \begin{bmatrix} v'_d \\ v'_q \end{bmatrix} \tag{3.20}$$

v_d and v_q is the input of the filter and v'_d and v'_q is the output of the filter. The relationship between v_d, v_q, v'_d and v'_q is shown in equation 3.21.

$$\begin{aligned} v'_d(s) &= \frac{v_d(s)}{\tau_d s + 1} \\ v'_q(s) &= \frac{v_q(s)}{\tau_q s + 1} \end{aligned} \tag{3.21}$$

Whereτ_d and τ_q are the time constants of the two first-order filters.

Combining equation, the state matrix and gain vector can be obtained.

$$\frac{d}{dt}\begin{bmatrix} v'_d \\ v'_q \end{bmatrix} = \begin{bmatrix} -\frac{\sin^2\hat{\theta}}{\tau_d} & -\frac{\sin\hat{\theta}\cos\hat{\theta}}{\tau_d} \\ -\frac{\sin\hat{\theta}\cos\hat{\theta}}{\tau_q} & -\frac{\cos^2\hat{\theta}}{\tau_q} \end{bmatrix} \begin{bmatrix} v'_d \\ v'_q \end{bmatrix} + \begin{bmatrix} \frac{\sin\hat{\theta}}{\tau_d} \\ \frac{\cos\hat{\theta}}{\tau_q} \end{bmatrix} v_\alpha \tag{3.22}$$

Let $\hat{\theta} = \hat{\omega}t + \hat{\phi}, v_\alpha = V\cos(\omega t + \phi)$, where $\hat{\phi}$ is the phase difference. Assume the estimated input frequency is the same as the real input frequency. The steady state output of the PD, $\bar{V}'_d$ and $\bar{V}'_q$ can be obtained by zeroing the derivative terms.

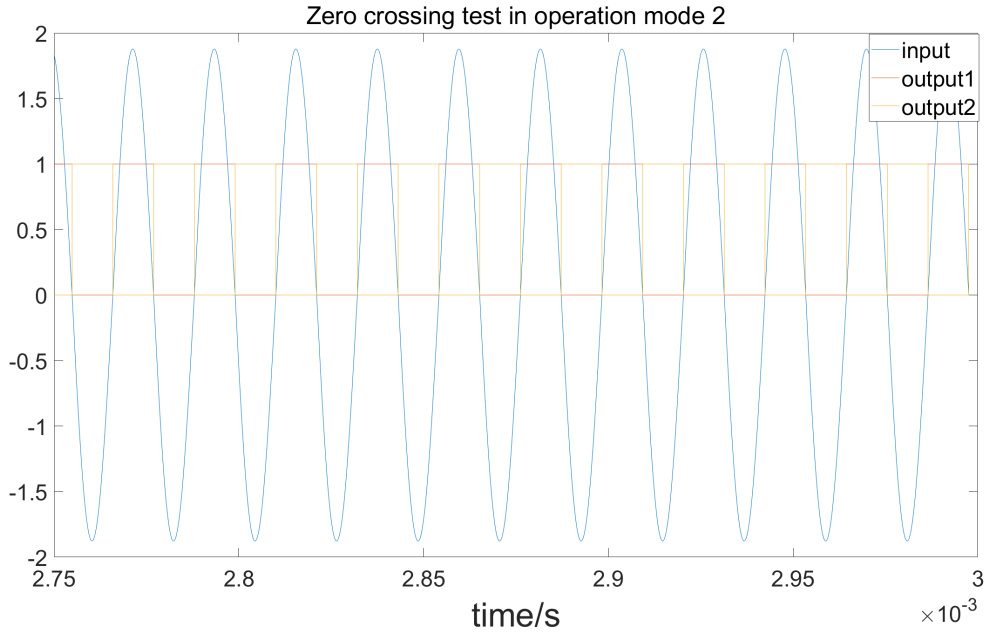

Figure 3.6: Input and output of zero crossing in operation mode 2

$$\begin{aligned} \bar{V}_d' &= V \sin \phi_e \\ \bar{V}_q' &= V \cos \phi_e \end{aligned} \tag{3.23}$$

Where $\phi_e = \hat{\phi} - \phi$. Assume the estimated angular frequency $\hat{\omega} \cong \omega$

According to the expression 3.23, ϕ_e will be zero if $\bar{V}_d'$ is zero. Besides, $\bar{V}_q'$ is the input voltage amplitude.
The differential equation for v_α' and v_β' is shown in equation 3.24.

$$\frac{d}{dt}\begin{bmatrix} v_\alpha' \\ v_\beta' \end{bmatrix} = \begin{bmatrix} -1/\tau & d\hat{\theta}/dt \\ -d\hat{\theta}/dt & 0 \end{bmatrix}\begin{bmatrix} v_\alpha' \\ v_\beta' \end{bmatrix} + \begin{bmatrix} 1/\tau \\ 0 \end{bmatrix} v_\alpha \tag{3.24}$$

Both of the time constant τ_d and τ_q are set as τ

Because of $d\hat{\theta}/dt$ is the definition of $\hat{\omega}$, the system can be regarded as a SISO linear time invariant system.

Therefore, the eigenvalue of the system can be represented as

$$\lambda_{1,2} = -\frac{1}{2\tau} \pm \frac{1}{2}\sqrt{\frac{1}{\tau^2} - 4\hat{\omega}^2} \tag{3.25}$$

According to this equation 3.25, the system is asymptotically stable to the point that the estimated angular frequency is equal to the real angular frequency. If the time constant is too small($\tau^{-1} \gg 2\hat{\omega}$), there will be two real solutions λ_1 and λ_2. The λ_1 will almost equal to $\tau^(-1)$ and λ_2 will be around zero and slow the dynamic characteristics of the system. If the time constant is too big($\tau^{-1} \ll 2\hat{\omega}$), there will be two complex conjugate solutions. The real part of these two values will be very small and will also slow the dynamic characteristics of the system.Therefore, the time constant of these two filters should be set as $1/(2\omega)$ to ensure the fast dynamic characteristics of the system.

The implementation in Simulink is shown in Figure 3.8.

The waveform of the frequency measurement of PLL unit is shown Figure 3.9 and 3.10. In operation mode 1, the measured frequency of the designed PLL unit is range from 50.4 kHz to 50.6 kHz. The average value of the measurement is 50.5 kHz. According to the formula 1.3, the reference value

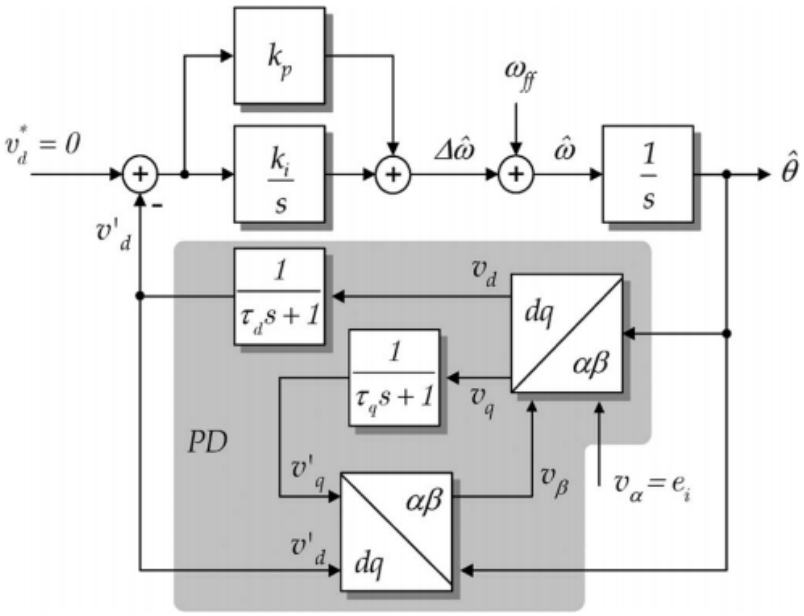

Figure 3.7: Topology of PLL

Table 3.3: Values of compared system parameters

Parameters	Values
Primary side DC voltage E_{DC}	10 V
Primary side compensation inductance L_p	362 μH
Secondary side compensation inductance L_s	155 μH
Primary side compensation capacitance C_1	27.7 nF
Primary side compensation capacitance C_2	4.8 nF
Secondary side compensation capacitance C_s	65.9 nF
Primary side resistance R_p	1.3 Ω
Secondary side resistance R_s	0.32 Ω

of the primary frequency in operation mode 1 is 50.6 kHz. Therefore, the error of the designed PLL unit is 0.198%.

In operation mode 2, the measured frequency of the designed PLL unit is range from 45.2 kHz to 45.4 kHz. The average value of the measurement is 45.3 kHz. According to the formula 1.3, the reference value of the primary frequency in operation mode 2 is 46.4 kHz. Therefore, the error of the designed PLL unit is 2.37%.

The waveform of the RMS measurement of PLL unit is shown in Figure 3.11 and 3.12.

3.4. Compared methodology

In order to compare the estimation accuracy of this methodology, a similar method based on the information from both the primary side and the secondary side is simulated in this subsection. The schematic of this method is shown in Figure 3.13 and 3.14.

Similar to the topology of the selected method, the circuit also consists of DC voltage source, full bridge inverter, winding, compensation capacitor and compensation inductance. The circuit schematic in Simulink is shown below. In order to control the variables, the circuit parameters are the same as the selected method. The zero crossing detection unit, PLL unit and RMS calculation unit are also the same as the selected method.

The circuit parameters are shown in Table 3.3.

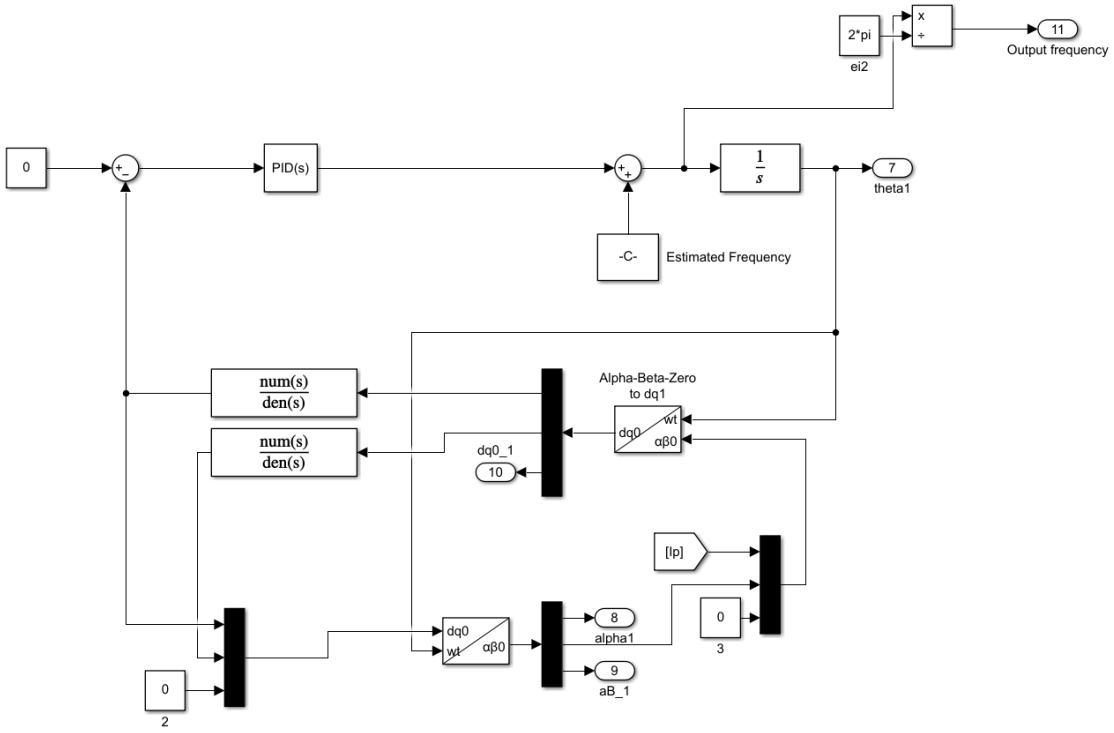

Figure 3.8: Topology of PLL unit

3.5. Results comparison and investigation

The result of the selected method and compared method will be shown in this section.

3.5.1. Load identification

In compared methodology, the load is known parameters. Therefore, only load identification of the selected method is implemented. The waveform of the load identification is shown in Figure 3.15. The real value of the load, the average value of the load identification unit and the error are shown in Table 3.4.

Table 3.4: Load identification result

Real value Ω	Identified value Ω	Error
10	9.7057	2.943%

3.5.2. Mutual inductance identification

The waveform of the mutual inductance identification of the selected method is shown in Figure 3.16. The waveform of the mutual inductance identification of the compared method is shown in Figure 3.17. The real value of the mutual inductance, the average value of the mutual inductance identification unit and the error are shown in Table 3.5.

According to the result of the selected method and compared method, the selected method has better performance in the accuracy of mutual inductance identification.

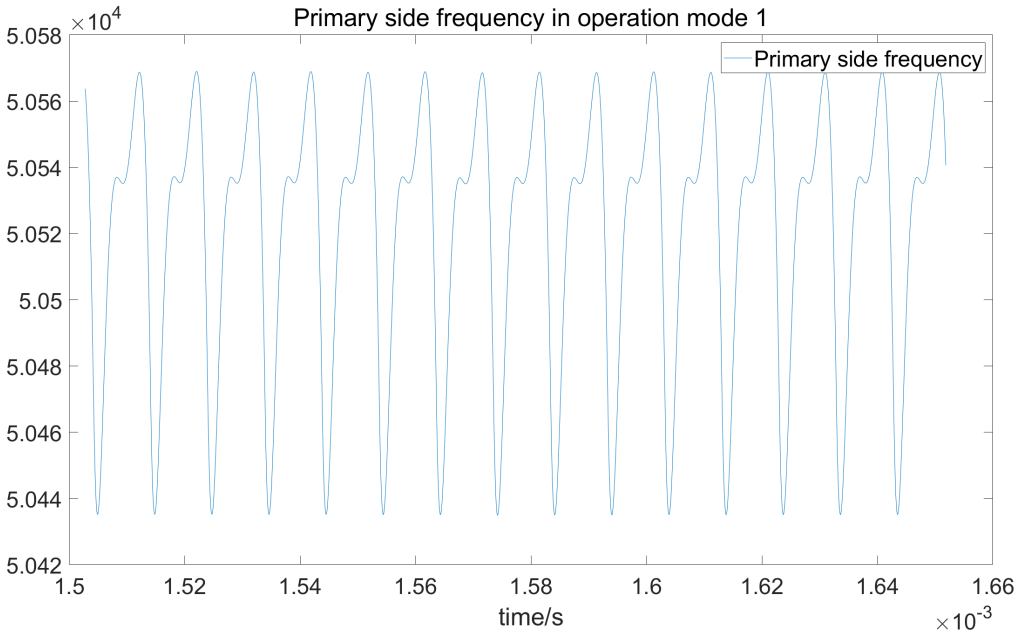

Figure 3.9: Frequency measurement of PLL unit in operation mode 1

Table 3.5: Mutual inductance identification result

	Real value μH	Identified value μH	Error
Selected method	35	35.382	1.09%
Compared method	35	37.203	6.29%

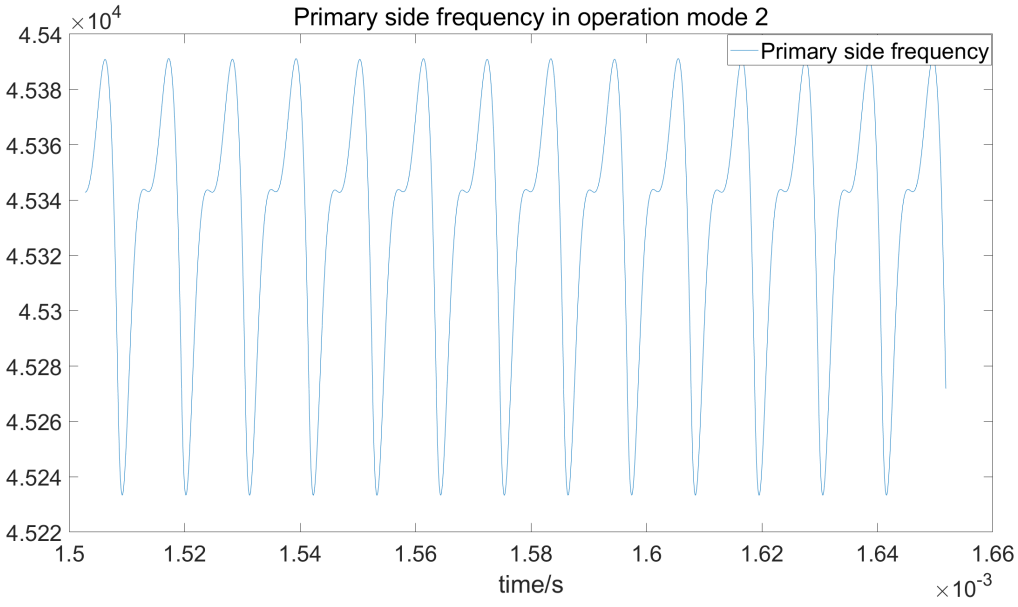

Figure 3.10: Frequency measurement of PLL unit in operation mode 2

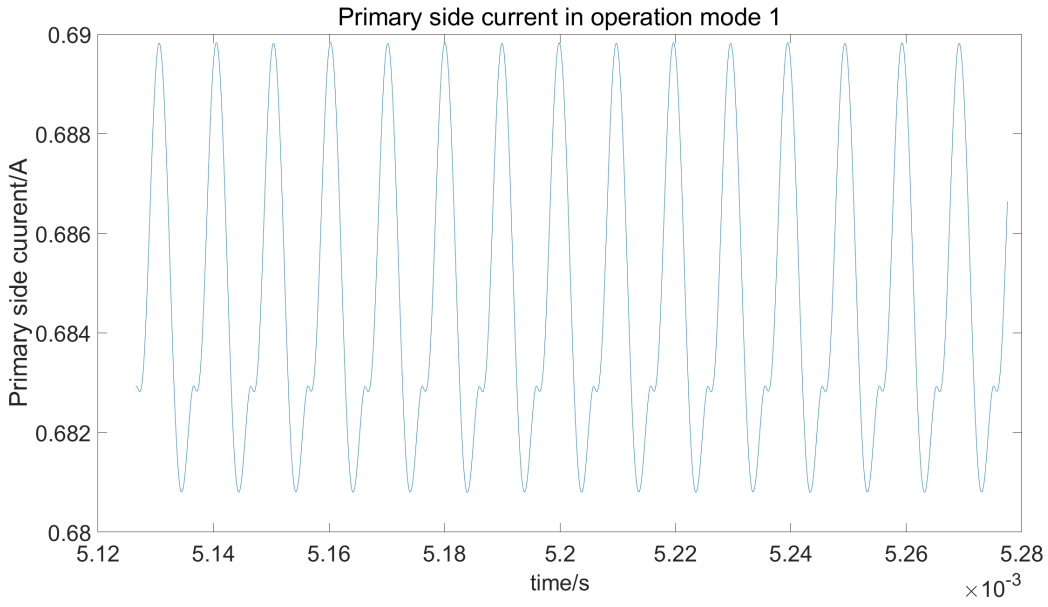

Figure 3.11: RMS measurement of PLL unit in operation mode 1

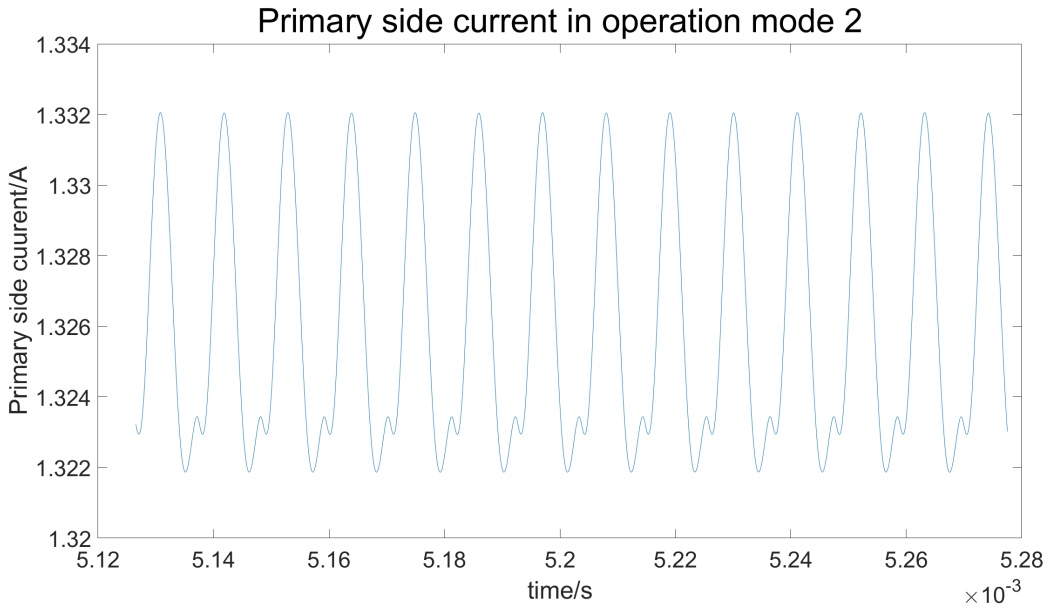

Figure 3.12: RMS measurement of PLL unit in operation mode 2

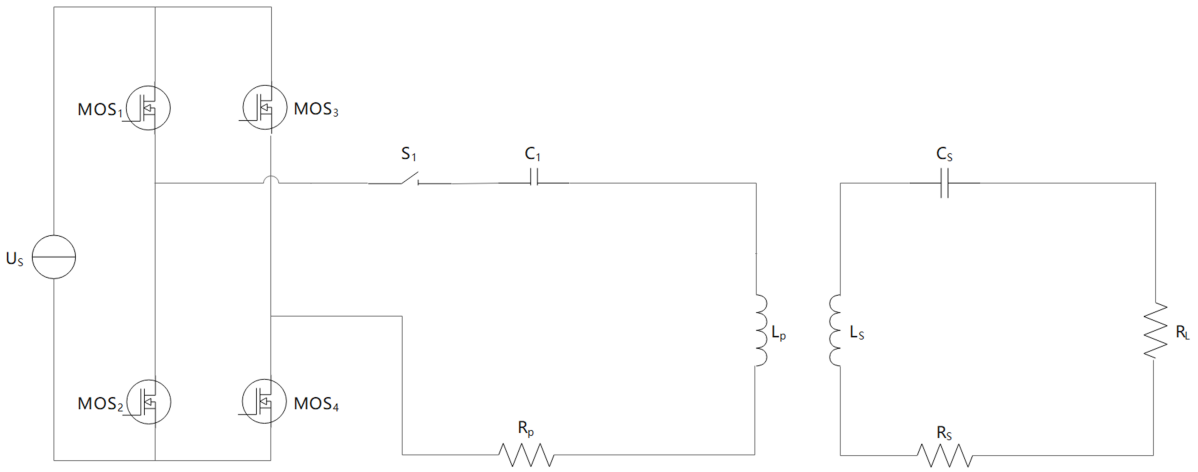

Figure 3.13: Circuit topology

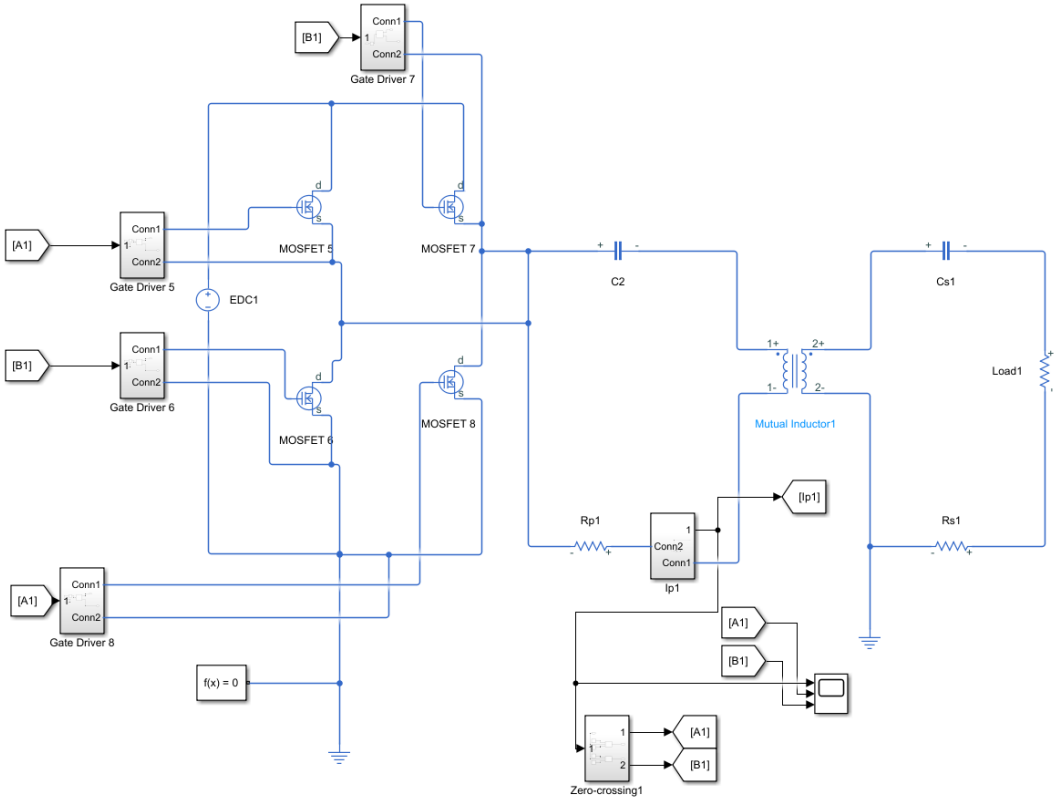

Figure 3.14: Circuit schematic in Simulink

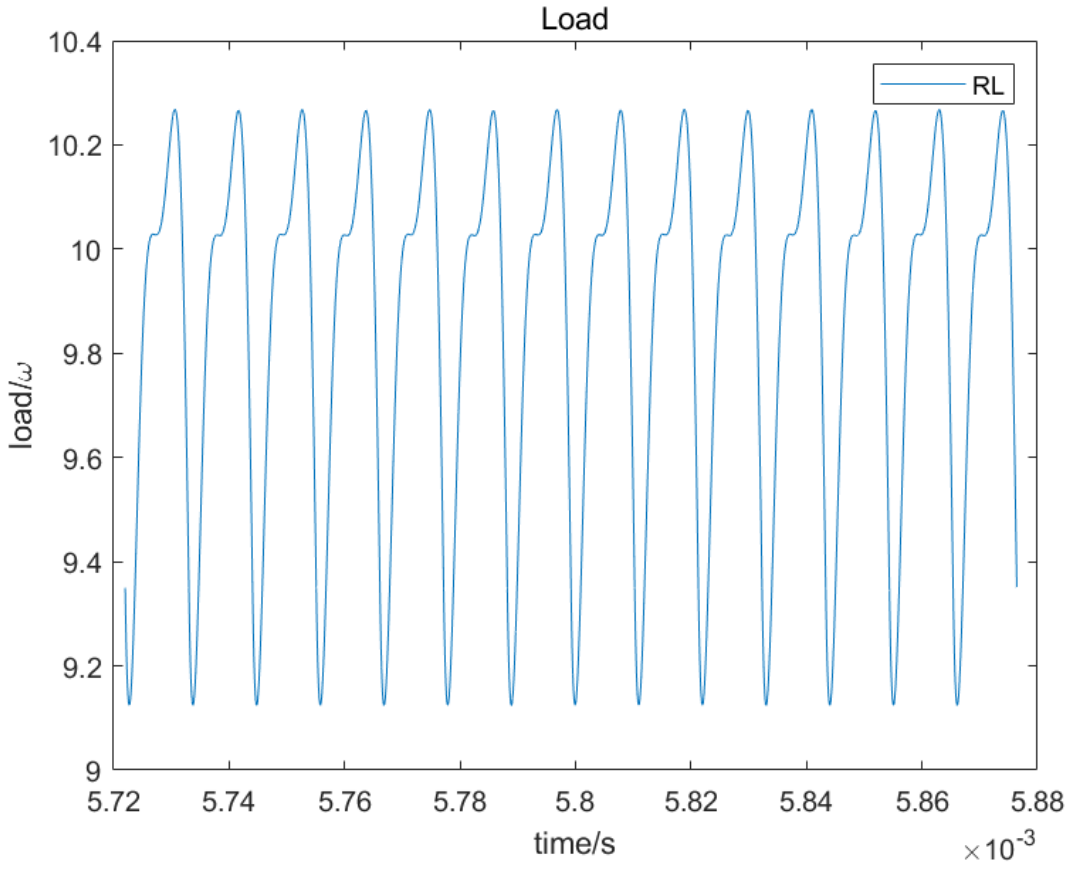

Figure 3.15: Load identification

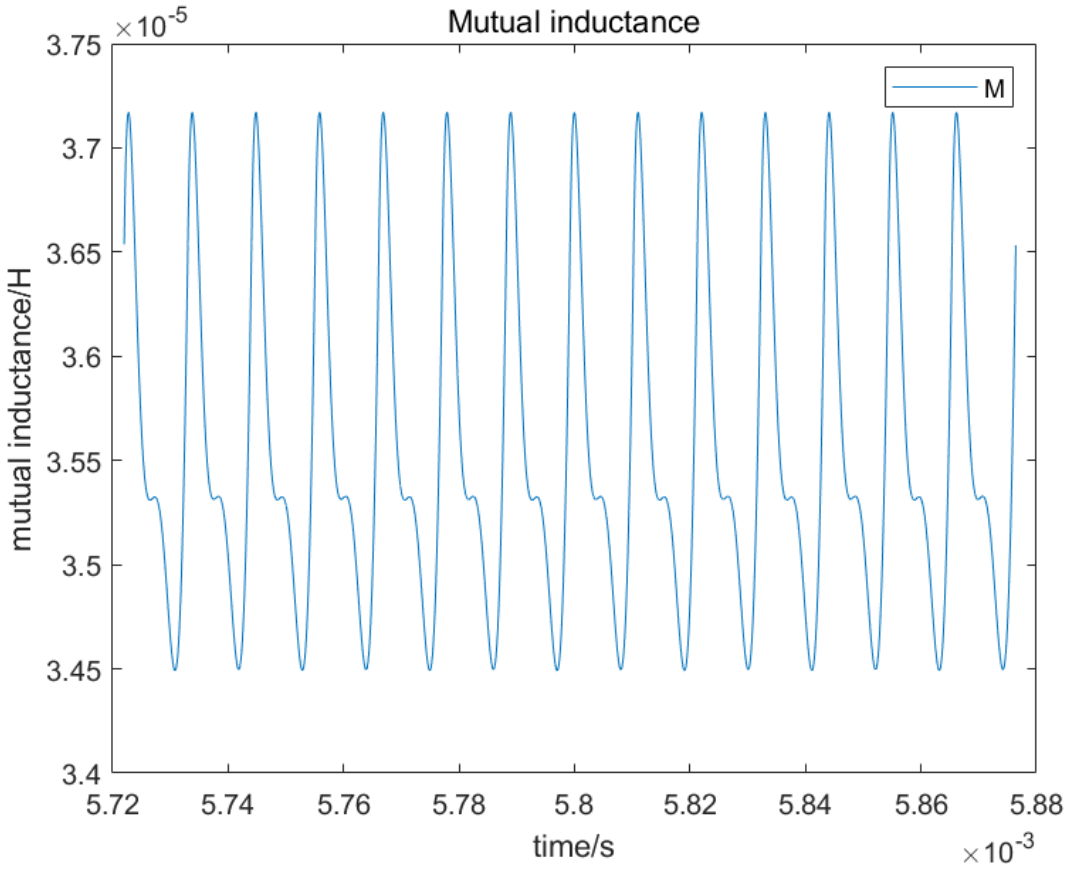

Figure 3.16: Mutual inductance identification of the selected method

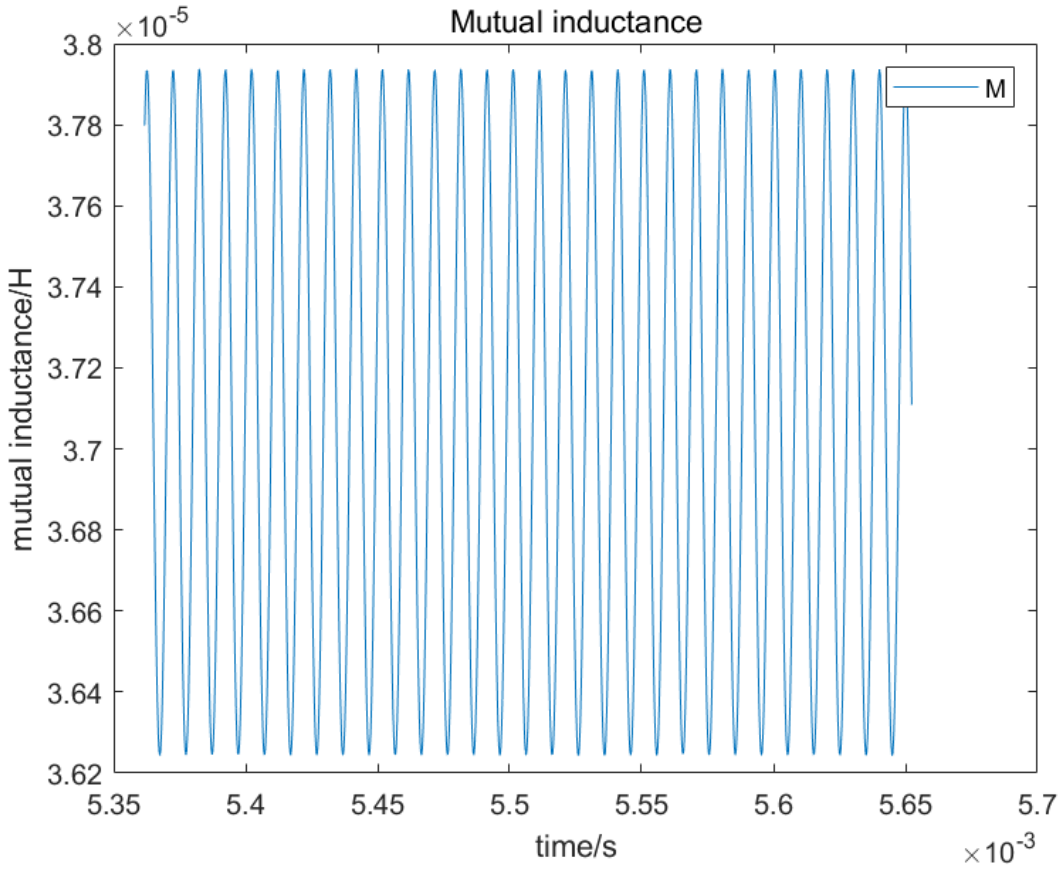

Figure 3.17: Mutual inductance identification of the compared method

4

Sensitivity study

In reality, the circuit parameters will fluctuate due to circuit aging. Therefore, it is necessary to estimate the accuracy of the method 'switching capacitance' when the circuit parameters are not the same as the rated value.

In this chapter, the influence of each circuit parameter's fluctuation will be analyzed. The circuit is always operated in full resonant state.

For primary capacitance C_1:

Real value of C_1 /nF	Error of C_1	Identified value of M /μH	Error of M	Identified value of load /Ω	Error of load
24.93	-10%	32.251i	-	-7.8279	-
26.315	-5%	1.2e-4 + 4.6e-5i	-	68.3673	-
27.7	0	35.382	1.09%	9.7057	2.94%
29.085	5%	40.481	0.71%	9.8371	1.35%
30.47	10%	49.942	1.11%	9.9201	2.21%

The deviation of the primary capacitance C_1 makes the system unstable. The reason is that the difference of the C_1 makes the operating frequency of the WPT system deviate from the expected frequency. The frequency detection unit and RMS detection unit can detect the respective frequency and RMS value. However, the load identification unit and mutual inductance identification unit will still use the default value of the circuit parameter. Therefore, the system will become unstable.

In order to ensure the stability of the system, the circuit parameters should be uploaded to the load identification unit and mutual inductance identification unit. The table below shows the identified value and accuracy of load identification and mutual inductance identification when the deviation of C_1 is uploaded to the identification unit.

Real value of C_1 /nF	Error of C_1	Identified value of M /μH	Error of M	Identified value of load /Ω	Error of load
24.93	-10%	35.097	1.10%	9.5989	4.01%
26.315	-5%	35.23	1.41%	9.5689	4.31%
27.7	0	35.382	1.09 %	9.7057	2.94%
29.085	5%	35.634	1.35%	9.8371	1.63%
30.47	10%	35.776	2.21%	9.9201	0.80%

According to the table, the accuracy of load identification and mutual inductance identification remain about 98%.

For primary capacitance C_2:

Real value of C_2 /nF	Error of C_2	Identified value of M /μH	Error of M	Identified value of load /Ω	Error of load
4.32	-10%	37.674	6.478%	14.3813	48.174%
4.56	-5%	35.964	1.928%	11.5961	19.477%
4.8	0	35.382	1.09%	9.7057	2.94%
5.04	5%	35.461	0.223%	8.3497	13.971%
5.28	10%	36.402	1.865%	7.2971	24.816%

Similar to the primary side C_1, the deviation of C_2 also makes the system unstable. However, it has less influence compared with C_1. The reason is that the value of C_1 is larger than C_2. Similar to the C_1, the table below shows the accuracy of load and mutual inductance when the deviation of C_2 is uploaded to the identification unit.

Real value of C_2 /nF	Error of C_2	Identified value of M /μH	Error of M	Identified value of load /Ω	Error of load
4.32	-10%	35.372	1.06%	9.7186	2.81%
4.56	-5%	35.401	1.15%	9.7573	2.43%
4.8	0	35.382	1.09%	9.7057	2.94%
5.04	5%	35.506	1.45%	9.7538	2.46%
5.28	10%	35.526	1.50%	9.7631	2.37%

The accuracy of load identification and mutual inductance identification is higher than 97% when the deviation of C_2 is uploaded to the identification unit.

For secondary capacitance C_s:

Real value of C_s /nF	Error of C_s	Identified value of M /μH	Error of M	Identified value of load /Ω	Error of load
59.31	-10%	28.802i	21.666%	5.839	39.839%
62.605	-5%	31.129	12.020%	7.4026	23.729%
65.9	0%	35.382	1.09%	9.7057	2.94%
69.195	5%	41.287	16.689%	13.3725	37.780%
72.49	10%	51.993	46.948%	21.6607	123.175%

Similar to the C_1, the deviation of C_s also makes the system become unstable. According to formula 3.8, the deviation of C_s will not influence the value of $ImZr$. Therefore, different from C_1, the deviation of C_s will not make the load identification become a negative value. The mutual inductance identification will not be calculated as a complex value. The table below shows the accuracy of load and mutual inductance when the deviation of C_s is uploaded to the identification unit.

Real value of C_s /nF	Error of C_s	Identified value of M /μH	Error of M	Identified value of load /Ω	Error of load
59.31	-10%	34.536	1.33%	9.8794	1.22%
62.605	-5%	35.38	1.09%	9.7666	2.33%
65.9	0%	35.382	1.09%	9.7057	2.94%
69.195	5%	35.007	0.02%	9.5031	4.97%
72.49	10%	34.005	2.7%	9.1063	8.94%

The accuracy of load identification is higher than 90 % when the deviation of C_s is uploaded to the identification unit. However, when the deviation of C_s is around 5 %, the accuracy of mutual inductance identification is around 81 %. The reason is the value of C_s is higher than C_1, therefore, the error of the identification value will be larger.

For primary inductance L_p:

Real value of L_p /μH	Error of L_p	Identified value of M /μH	Error of M	Identified value of load /Ω	Error of load
325.8	-10%	28.802i	-	-5.309	-
343.9	-5%	122.88i	-	-203.128	-
362	0	35.382	1.09%	9.7057	2.94%
380.1	5%	35.643	0.74%	9.8511	1.49%
398.2	10%	35.79	1.15%	9.9527	2.54%

The deviation of the primary inductance L_p will also makes the system unstable. Similar to the primary side capacitance, the difference of the L_p makes the system operating frequency of WPT system deviate. The frequency detection unit and RMS detection unit can detect the respective frequency and RMS value but the load identification unit and mutual inductance identification unit will still use the default value of the circuit parameters. Therefore, the system will become unstable. The table below shows the accuracy of load and mutual inductance when the deviation of L_p is uploaded to the identification unit.

Real value of L_p /μH	Error of L_p	Identified value of M /μH	Error of M	Identified value of load /Ω	Error of load
325.8	-10%	35.096	0.27%	9.522	4.78%
343.9	-5%	35.209	0.60%	9.6507	3.50%
362	0	35.382	1.09%	9.7057	2.94%
380.1	5%	35.643	1.84%	9.8511	1.49%
398.2	10%	35.79	2.26%	9.9527	0.46%

The accuracy of load identification and mutual inductance identification is higher than 97% when the deviation of L_p is uploaded to the identification unit.

For secondary inductance L_s:

Real value of L_s /μH	Error of L_s	Identified value of M /μH	Error of M	Identified value of load /Ω	Error of load
139.5	-10%	29.206	17.455%	6.5201	32.822%
147.25	-5%	31.868	9.932%	7.8256	19.371%
155	0	35.382	1.09%	9.7057	2.94%
162.75	5%	40.366	14.086%	12.7966	31.846%
170.5	10%	49.495	39.888%	19.5454	101.381%

Similar to C_s, the deviation of L_s will also make the system unstable. According to formula 3.8, the deviation of L_s will not influence the value of $ImZr$. Therefore, the deviation of L_s will keep the load identification as a positive value. The mutual inductance identification will remain a real value. The table below shows the accuracy of load and mutual inductance when the deviation of L_s is uploaded to the identification unit.

Real value of L_s /μH	Error of L_s	Identified value of M /μH	Error of M	Identified value of load /Ω	Error of load
139.5	-10%	35.609	1.74%	9.8378	1.62%
147.25	-5%	35.497	1.42%	9.808	1.92%
155	0	35.382	1.09%	9.7057	2.94%
162.75	5%	35.098	0.28%	9.5837	4.16%
170.5	10%	34.359	1.83%	9.2456	7.54%

The accuracy of mutual inductance identification is higher than 97% and the accuracy of load identification is higher than 90 % when the deviation of L_s is uploaded to the identification unit.

For primary resistance R_p:

Real value of R_p /Ω	Error of R_p	Identified value of M /μH	Error of M	Identified value of load /Ω	Error of load
1.17	-10%	34.897	1.371%	9.5006	4.99%
1.235	-5%	35.118	0.746%	9.6324	3.68%
1.3	0	35.382	1.09%	9.7057	2.94%
1.365	5%	35.577	0.551%	9.8611	1.389%
1.43	10%	35.81	1.195%	9.9739	0.26%

The primary side resistance R_p has minimal impact on mutual inductance identification and load identification. The value of R_p varies from 90% to 110%, while the error of mutual inductance identification is less than 1.5 % and the error of load identification is less than 3%.

For secondary resistance R_s:

Real value of R_s /Ω	Error of R_s	Identified value of M /μH	Error of M	Identified value of load /Ω	Error of load
0.288	-10%	35.382	1.09%	9.4359	5.641%
0.304	-5%	35.382	1.09%	9.4199	5.801%
0.32	0	35.382	1.09%	9.7057	2.94%
0.336	5%	35.382	1.09%	9.3879	6.121%
0.352	10%	35.382	1.09%	9.3719	6.281%

Similar to the primary side resistance R_p, the secondary side resistance R_s also have little effect to load identification. Due to the expression of R_L,

$$R_L = \frac{\left(0.9E_{\mathrm{DC}} - I_{p2}R_p\right)\cdot\left(\frac{1}{\omega_2 C_s} - \omega_2 L_s - \omega_2 L\right)}{\mathrm{Im}\, Z_{r2}\cdot I_{p2}} - R_s \tag{4.1}$$

The error of the R_L will be the same as the error of the R_s. According to the expression of M,

$$ReZs = R_L + R_s M = \sqrt{\frac{\mathrm{Im}\, Z_{r2}\left[ReZ_s^2 + \left(\frac{1}{\omega_2 C_s} - \omega_2 L_s\right)^2\right]}{\omega_2^2\left(\frac{1}{\omega_2 C_s} - \omega_2 L_s\right)}} \tag{4.2}$$

The error of the R_s will be balanced so that it do not affect the identification of mutual inductance.

For load R_L:
In real life, different load is the most common scenario. In this case, the load is set to vary from 50%

Real value of Load /Ω	Identified value of M	Error of M	Identified value of load /Ω	Error of load
5	35.604	1.726%	5.0001	0.002%
10	35.382	1.09%	9.7057	2.94%
15	34.783	0.62%	14.0729	6.18%
20	34.194	2.303%	18.1983	9.01%
30	33.508	4.263%	26.5437	11.521%

to 300 % while the errors of the mutual inductance are always under 5% and the errors of the load are no more than 12%.

5

Summary and future work

With the population of EVs, the demand of vehicle charging is also increasing. As an innovative charging method, wireless power transfer can avoid some safety issues compared with traditional vehicle charging. The coupling factor is one of the most important parameters of the wireless power transfer system. In order to optimize the transfer efficiency, estimating the coupling factor accurately is necessary. The objective of this work is to review and classify existing methodologies of coupling factor estimation. Besides, comparison in simulation tools are implemented. In simulation chapter, the implementation of zero-crossing unit and PLL unit are implemented.

5.1. Summary

In Chapter 1, the background of the WPT system is introduced. Besides, the equivalent circuit of the WPT system is analyzed. Based on the circuit analysis, the influence of the coupling factor is studied. The research objectives are also proposed in this chapter.
In Chapter2, the existing methodologies of coupling factor are reviewed. Six different methodologies are analyzed and concluded.
Chapter 3 made a detailed analysis of one methodology that uses alternative primary side capacitance. Simulation in Simulink is implemented. The zero-crossing unit and PLL unit are designed and tested. Besides, another methodology is also simulated and compared in this chapter. The selected method has better accuracy compared with another method.
In Chapter 4, the sensitivity of the system is tested. The circuit parameter will fluctuate from 95% to 105%. The system work in stable status when the primary side resistance, secondary side resistance or load fluctuate. However, the system will become unstable when the value of primary side capacitance, primary side inductance, secondary side capacitance and secondary side inductance fluctuate. The reason is that the frequency detection unit and RMS detection unit can detect the deviation, however, the load identification unit and mutual inductance identification unit will use the default value. Therefore, the estimation of mutual inductance and load will have a huge derivation. Once the deviation of the circuit parameter is uploaded to the load identification unit and mutual inductance identification unit, the accuracy of the system will remain at a high level.

5.2. Future work

There are still some future works about this thesis.
First, according to the sensitivity study, the system will become unstable because of the derivation of the primary side capacitance, primary side inductance and secondary side inductance. In reality, the derivation of circuit parameters is common. Therefore, capacitance and inductance identification unit is necessary.
Second, this thesis only considers the load as pure resistance. However, in reality, the load may consists of external inductance and capacitance. The methodology is available when the load consists of external inductance. But in the simulation, this part is not implemented.
Third, this methodology only considers static wireless power transfer. However, the dynamic WPT system is also required. More further works need to be done on dynamic wireless charging.

Bibliography

[1] S. Sasikumar and K. Deepa, “Comparative study of lcl-s and lcc-s topology of wireless ev charging system,” in *2019 Innovations in Power and Advanced Computing Technologies (i-PACT)*, vol. 1, 2019, pp. 1–6. DOI: 10.1109/i-PACT44901.2019.8960121.

[2] A. Marinescu, I. Dumbrava, A. Vintilă, *et al.*, “The way to engineering ev wireless charging: Dacia electron,” in *2017 Electric Vehicles International Conference (EV)*, 2017, pp. 1–6. DOI: 10.1109/EV.2017.8242094.

[3] D. Pedder, A. Brown, and J. Skinner, “A contactless electrical energy transmission system,” *IEEE Transactions on Industrial Electronics*, vol. 46, no. 1, pp. 23–30, 1999. DOI: 10.1109/41.744372.

[4] C.-S. Wang, O. Stielau, and G. Covic, “Design considerations for a contactless electric vehicle battery charger,” *IEEE Transactions on Industrial Electronics*, vol. 52, no. 5, pp. 1308–1314, 2005. DOI: 10.1109/TIE.2005.855672.

[5] H. Yang, Y. Gao, K. B. Farley, M. Jerue, J. Perry, and Z. Tse, “Ev usage and city planning of charging station installations,” in *2015 IEEE Wireless Power Transfer Conference (WPTC)*, 2015, pp. 1–4. DOI: 10.1109/WPT.2015.7139139.

[6] M. A. Yousuf, T. K. Das, M. E. Khallil, N. A. A. Aziz, M. J. Rana, and S. Hossain, “Comparison study of inductive coupling and magnetic resonant coupling method for wireless power transmission of electric vehicles,” in *2021 2nd International Conference on Robotics, Electrical and Signal Processing Techniques (ICREST)*, 2021, pp. 737–741. DOI: 10.1109/ICREST51555.2021.9331096.

[7] Z. Despotovic, V. Vasic, D. Oros, and D. Jerkan, “Coupling factor estimation in vehicle-to-vehicle wireless power transfer system based on geometry properties,” in *2020 IEEE Wireless Power Transfer Conference (WPTC)*, 2020, pp. 227–230. DOI: 10.1109/WPTC48563.2020.9295617.

[8] IEC61980-1, “Electric vehicle wireless power transfer (WPT) systems - part 1:General requirements,” IEC, Standard, Jul. 2015.

[9] International Commission on Non□Ionizing Radiation Protection, “ICNIRP guidelines for limiting exposure to time□varying electric and magnetic fields (1Hz–100kHz),” ICNIRP, Standard, 2010.

[10] ISO/PAS19363:2017, “Electrically propelled road vehicles - magnetic field wireless power transfer - Safety and interoperability requirements,” ISO, Standard, Jan. 2017.

[11] J2954RP, “Wireless power transfer for Light-Duty Plug-In/ Electric Vehicles and Alignment Methodology,” SAE International, Standard, Apr. 2019.

[12] W. Zhang and C. C. Mi, “Compensation topologies of high-power wireless power transfer systems,” *IEEE Transactions on Vehicular Technology*, vol. 65, no. 6, pp. 4768–4778, 2016. DOI: 10.1109/TVT.2015.2454292.

[13] H. Movagharnejad and A. Mertens, “Design metrics of compensation methods for contactless charging of electric vehicles,” in *2017 19th European Conference on Power Electronics and Applications (EPE’17 ECCE Europe)*, 2017, P.1–P.10. DOI: 10.23919/EPE17ECCEEurope.2017.8099403.

[14] Z. U. Zahid, C. Zheng, R. Chen, *et al.*, “Design and control of a single-stage large air-gapped transformer isolated battery charger for wide-range output voltage for ev applications,” in *2013 IEEE Energy Conversion Congress and Exposition*, 2013, pp. 5481–5487. DOI: 10.1109/ECCE.2013.6647445.

[15] H. Li, J. Li, K. Wang, W. Chen, and X. Yang, “A maximum efficiency point tracking control scheme for wireless power transfer systems using magnetic resonant coupling,” *IEEE Transactions on Power Electronics*, vol. 30, no. 7, pp. 3998–4008, 2015. DOI: 10.1109/TPEL.2014.2349534.

[16] X. Zhang, J. Wang, M. Xue, Y. Li, and Q. Yang, “Reserch on dynamic wireless charging of electric vehicle based on double lcc compensation mode,” in *2019 IEEE Wireless Power Transfer Conference (WPTC)*, 2019, pp. 141–145. DOI: 10.1109/WPTC45513.2019.9055681.

[17] K. Stoyka, G. Di Capua, G. Di Mambro, *et al.*, “Behavioral models for the analysis of dynamic wireless charging systems for electrical vehicles,” in *2020 IEEE International Symposium on Circuits and Systems (ISCAS)*, 2020, pp. 1–5. DOI: 10.1109/ISCAS45731.2020.9180785.

[18] S. L. W.H. Ko and C. Fung, “Design of radio-frequency powered coils for implant instruments,” *Medical Biological Engineering Computing*, vol. 15, no. 6, pp. 634–640, 1977.

[19] Y.-G. Su, H.-Y. Zhang, Z.-H. Wang, A. Patrick Hu, L. Chen, and Y. Sun, “Steady-state load identification method of inductive power transfer system based on switching capacitors,” *IEEE Transactions on Power Electronics*, vol. 30, no. 11, pp. 6349–6355, 2015. DOI: 10.1109/TPEL.2015.2411755.

[20] J. P. W. Chow and H. S. H. Chung, “Use of primary-side information to perform online estimation of the secondary-side information and mutual inductance in wireless inductive link,” in *2015 IEEE Applied Power Electronics Conference and Exposition (APEC)*, 2015, pp. 2648–2655. DOI: 10.1109/APEC.2015.7104725.

[21] K. Hata, T. Imura, and Y. Hori, “Simultaneous estimation of primary voltage and mutual inductance based on secondary-side information in wireless power transfer systems,” in *2016 IEEE Wireless Power Transfer Conference (WPTC)*, 2016, pp. 1–3. DOI: 10.1109/WPT.2016.7498763.

[22] V. Jiwariyavej, T. Imura, and Y. Hori, “Coupling coefficients estimation of wireless power transfer system via magnetic resonance coupling using information from either side of the system,” *IEEE Journal of Emerging and Selected Topics in Power Electronics*, vol. 3, no. 1, pp. 191–200, 2015. DOI: 10.1109/JESTPE.2014.2332056.

[23] X. Dai, X. Li, Y. Li, and A. P. Hu, “Maximum efficiency tracking for wireless power transfer systems with dynamic coupling coefficient estimation,” *IEEE Transactions on Power Electronics*, vol. 33, no. 6, pp. 5005–5015, 2018. DOI: 10.1109/TPEL.2017.2729083.

[24] R. M. Santos Filho, P. F. Seixas, P. C. Cortizo, L. A. B. Torres, and A. F. Souza, “Comparison of three single-phase pll algorithms for ups applications,” *IEEE Transactions on Industrial Electronics*, vol. 55, no. 8, pp. 2923–2932, 2008. DOI: 10.1109/TIE.2008.924205.